



FeNi bimetallic functionalized lignin catalyst for sustainable oxidation processes

Mehdi Mennani^{a,*}, Youness Abdellaoui^{b,*}, Anass Ait Benhamou^c,
Eduardo Alberto Lopez-Maldonado^d, Meriem Kasbaji^a, Mounir El Achaby^a, Amine Moubarik^e,
Zineb Kassab^{a,*}

^a Materials Science, Energy and Nanoengineering (MSN) Department, Mohammed VI Polytechnic University, Lot 660 – Hay Moulay Rachid, 43150 Ben Guerir, Morocco

^b CONAHCyT-Cinvestav Saltillo. Sustainability of Natural Resources and Energy, Coahuila, Mexico, Av. Industria Metalúrgica 1062, Parque Industrial Ramos Arizpe, Ramos Arizpe, Coahuila C.P. 25900, Mexico

^c Department of Wood and Forest Sciences, Renewable Materials Research Centre (CRMR), Université Laval, Quebec, QC G1V 0A6, Canada

^d Faculty of Chemical Sciences and Engineering, Autonomous University of Baja California, CP, Tijuana 22424, Tijuana B.C., Mexico

^e Chemical Processes and Applied Materials Laboratory, Polydisciplinary Faculty, Sultan Moulay Slimane University, BP 592, Beni Mellal, Morocco

ARTICLE INFO

Keywords:

Lignin
Biomass
Biopolymer catalyst
Oxidation
Cellulose
Bimetallic catalyst
Sustainability

ABSTRACT

The advancement of sustainable and efficient catalytic procedures is crucial in tackling the continuous environmental and industrial challenges, with research being inherently focused on sustainable chemical science to exploit the possibilities of cost-effective bio-based materials for practical applications. Considerably, this investigation delves into the synthesis, characterization, and use of Fe–Ni bimetallic functionalized lignin (FeNi@Lig) catalysts using lignin extracted from spent coffee grounds, an underutilized agro-industrial waste. This eco-friendly approach emphasizes the valorization of non-traditional biomass while reducing waste streams. FeNi@Lig was used for oxidation processes, concentrating on the oxidation of bromothymol blue and cellulose for environmental remediation and the production of valuable chemicals. By capitalizing on the multifaceted attributes of lignin, FeNi@Lig catalysts were produced and examined using several techniques, uncovering an effective dispersion of Fe and Ni nanoparticles on the lignin support. The catalysts displayed remarkable efficiency and selectivity in oxidative processes, notably boosting reaction speeds and diminishing the creation of unwanted side products. The oxidation of bromothymol blue (BB) was carried out with a 2 % catalyst, yielding a conversion efficiency of 99.35 % in just 180 s. Likewise, the optimal cellulose oxidation exhibited an oxidation degree of 91.11 % with a 5 % catalyst. The outcomes emphasize the promise of catalysts derived from biomass in industrial settings, advocating for sustainable methodologies and propelling the realm of eco-friendly chemistry.

1. Introduction

The significant rise in demand for efficient and sustainable catalytic processes in recent years can be attributed to the rapid industrialization and urbanization that has taken place. Catalysts play a vital role in a variety of chemical reactions, such as hydrogenation [1], dehydrogenation [2], and the breakdown of organic pollutants [3], which are

essential in the production of chemicals, fuels, and valuable materials within the industrial sector. Nevertheless, conventional catalysts often depend on precious metals, leading to high costs and environmental issues. Consequently, there has been a shift towards investigating alternative materials that are abundant, cost-effective, and environmentally friendly for catalytic purposes [4,5]. One such material showing promise is lignin, a complex aromatic polymer present in plant

Abbreviations: BB, Bromothymol Blue; BET, Brunauer-Emmett-Teller; COOH, Carboxyl Group; DO, Degree of Oxidation; DW, Distilled Water; EDX, Energy-Dispersive X-ray Spectroscopy; FeNi@Lig, Iron-Nickel Bimetallic Catalyst Supported on Lignin; FTIR, Fourier Transform Infrared Spectroscopy; H₂O₂, Hydrogen Peroxide; HGS, Hydroxy-Guaiacyl-Syringyl Lignin Units; NaOH, Sodium Hydroxide; OC, Oxidized Cellulose; OER, Oxygen Evolution Reaction; OH, Hydroxyl Group; RC, Raw Cellulose; RHE, Reversible Hydrogen Electrode; SCG, Spent Coffee Grounds; SEM, Scanning Electron Microscopy; TGA, Thermogravimetric Analysis; TOF, Turnover Frequency; UOR, Urea Oxidation Reaction; UV-Vis, Ultraviolet-Visible Spectroscopy; XPS, X-ray Photoelectron Spectroscopy; XRD, X-ray Diffraction.

* Corresponding authors.

E-mail addresses: mehdi.mennani@um6p.ma (M. Mennani), youness@cinvestav.mx (Y. Abdellaoui), zineb.kassab@um6p.ma (Z. Kassab).

<https://doi.org/10.1016/j.susmat.2025.e01267>

Received 31 October 2024; Received in revised form 2 January 2025; Accepted 19 January 2025

Available online 21 January 2025

2214-9937/© 2025 The Authors. Published by Elsevier B.V. This is an open access article under the CC BY-NC license (<http://creativecommons.org/licenses/by-nc/4.0/>).

cell walls and a major byproduct of the paper and biofuel industries. Despite being commonly considered as waste and usually incinerated for energy retrieval, lignin's distinctive chemical composition, characterized by a high content of aromatic rings and functional groups (OH, COOH, OCH₃, C=O, etc.), renders it an appealing option for functionalization and utilization in catalysis [6–9].

The combined influence of Fe and Ni possesses the potential to augment catalytic performance, thereby augmenting the value of these materials in diverse catalytic processes. Worth mentioning that Iron (Fe) is recognized for its reactivity and capacity to trigger hydrogen, making it valuable in hydrogenation reactions. Conversely, Nickel (Ni) contributes stability and enhances the activity of iron. When these two metals are combined, their interaction generates a synergistic effect that enhances their overall catalytic efficiency [10–12]. Fang et al. [13] synthesized FeNi-N/C, exhibiting considerable efficacy in oxygen reduction reactions (ORR) under alkaline environments, with an observed onset potential of 0.965 V relative to the reversible hydrogen electrode (RHE). The investigation underscored the synergistic interaction between Fe and Ni, identifying Fe-Nx-C as the predominant active site, which is further augmented by the incorporation of Ni-Nx-C, thereby enhancing ORR efficacy. FeNi/NiFe₂O₄@NC catalyst that integrates pyridinic N-doped carbon layers with tensile stress to improve water oxidation (OER) and urea oxidation (UOR) performance. The catalyst showed outstanding OER activity with an overpotential of 196 mV at 100 mA/cm², and exceptional UOR performance with a potential of 1.32 V at 10 mA/cm². It retained its stability at 1000 mA/cm² for OER in 6.0 mol/L KOH and at 500 mA/cm² for UOR in 1.0 mol/L KOH with 0.33 mol/L urea for 50 h [14]. Noteworthy, in heterogeneous catalysis, unsupported Ni and Fe can leach into the reaction medium, reducing reusability and contaminating products. Besides, metal nanoparticles tend to aggregate, reducing available active sites and overall efficiency [5,15]. Considerably, by incorporating the Fe–Ni bimetallic system into the lignin structure, a material with improved catalytic activity and stability can be achieved.

Utilizing lignin as a foundation for Fe–Ni bimetallic catalysts not only enhances the value of this abundant biopolymer but also adheres to the principles of green chemistry. By transforming lignin into high-performance catalytic materials, it becomes feasible to minimize waste generation and encourage the sustainable utilization of biomass resources [16,17]. Furthermore, the inherent characteristics of lignin, such as its thermal stability and capacity to establish strong bonds with metal nanoparticles, make it an excellent support for catalytic applications [18–20]. Researchers have examined lignin-based catalysts owing to their promise as environmentally benign and plentiful resources. Nevertheless, the intricate and heterogeneous architecture of lignin, which fluctuates according to the biomass source and the method of isolation, presents significant obstacles to reproducibility and catalytic performance [17,21]. For example, prior investigations have underscored the challenges associated with attaining uniform functionalization of lignin, which may result in erratic distribution of active sites [17,22]. This complication adversely affects the overall catalytic efficacy, particularly in oxidation and hydrogenation processes. Furthermore, the interactions between metal nanoparticles and the lignin substrate have been less than optimal, culminating in the agglomeration of nanoparticles or their leaching during catalytic operations. Nezafat et al. [23] observed that, notwithstanding lignin's promise as a supportive matrix, the weak metal-lignin interactions frequently lead to diminished stability and recyclability of the catalyst.

The potential for catalytic oxidation utilizing different catalytic mechanisms stands as a pivotal realm of study, particularly within the context of environmental remediation and the chemical sector. Catalytic oxidation procedures play a vital role in converting pollutants and organic substrates into less harmful or more valuable outputs [24,25]. The oxidation of bromothymol blue, an organic dye commonly employed as a pH indicator, serves as a prime illustration. Bromothymol blue poses a persistent threat in aquatic environments, and its existence

in nature can be detrimental owing to its toxic attributes [26,27]. On the other hand, different catalytic systems have been investigated for their effectiveness in the oxidation of cellulose through varied methodologies. In a study by Li et al. [28] the Fenton reaction (H₂O₂ – FeSO₄) was employed to fabricate cellulose nanofibers through catalyzed oxidation. Another study by Tang et al. [29] documented the TEMPO-oxidized cellulose featuring a high degree of oxidation (91 %) achieved through a two-step process involving NaOH/urea and TEMPO/NaBr/NaClO system. Furthermore, Kageshima et al. [30] investigated the electrocatalytic oxidation of cellulose using Au, Pd, and Ni catalysts, resulting in the production of short-chain hydrocarbons and a transition of the crystalline structure from cellulose I to II, signifying the retention of the cellulose skeleton structure throughout these procedures.

Bio-based catalysts derived from lignin are gaining attention for catalytic oxidation applications. Most studies focus on traditional biomass sources, such as wood and agricultural by-products. In contrast, our study utilizes lignin from spent coffee grounds, an abundant agro-industrial by-product, to develop a novel Fe–Ni bimetallic catalyst. The Fe–Ni system combines iron's redox activity with nickel's stability, offering synergistic performance. Nevertheless, its implementation on a lignin substrate, particularly for high-efficiency oxidation under mild conditions, continues to be insufficiently investigated. As we delve deeper into exploring the synergy between biomass-derived materials and state-of-the-art catalytic systems, the approach delineated in our research underscores the synthesis, characterization, and utilization of innovative biopolymer functionalized bimetallic catalysts in oxidative conversions. Our approach highlights the potential of biomass-derived materials in sustainable catalytic processes, addressing environmental challenges and paving the way for industrial applications.

2. Experimental section

2.1. Chemicals and materials

The lignin used in this study was recovered from spent coffee (SC, *Coffea arabica* Linn) using an alkaline delignification process [31–33]. The initial step involved subjecting raw SC to hydrolysis using hot water to extract water-soluble components. The resultant soluble components were removed, leaving behind residues that were subsequently combined with a 15 % sodium hydroxide (NaOH) alkali solution and heated at 90 °C for 90 min, facilitating the dissolution of lignin into the alkali solution. The resulting mixture was filtered to segregate the dissolved lignin from the solid residue. The separated lignin was then precipitated using a diluted acid solution (5 M sulfuric acid, H₂SO₄) until reaching a pH of 2, followed by rinsing with ethanol and distilled water. Sulfuric acid was acquired from VWR Chemical. Hydrogen peroxide (H₂O₂, 30 %), nickel (II) sulfate NiSO₄(H₂O)₆, iron (III) sulfate hexahydrate FeSO₄, microcrystalline cellulose (C₆H₁₀O₅, 99 % purity), NaOH (99 %), HCl (37 %), ethanol, and bromothymol blue, were supplied by Sigma-Aldrich.

2.2. Bimetallic Fe–Ni@lignin preparation and catalytic application

The preparation of a lignin-derived Fe–Ni bimetallic catalyst (Fe–Ni@Lig) has been undertaken based on a modified reliable and efficient hydrothermal approach, enabling the embedding of metal catalysts on biopolymers [19,22,34]. Precisely, 5 g of dried isolated raw lignin (RL) was combined with 0.5 g of each metal powder (Fe and Ni) and mechanically shredded using a mortar grinder. The obtained powder was then mixed with 100 mL ethanol/water solution (1:1) and subjected to ultrasound for about 20 min to ensure impregnation and dispersion of the metals. The homogenized product underwent filtration, washing with distilled water (DW), drying, and direct carbonization in a tube furnace system under a nitrogen atmosphere with a flow rate of 10 mL/min. The annealing procedure involved a gradual temperature ramp from room temperature to 500 °C at a rate of 5 °C/min, maintaining this

temperature for 2 h. Subsequently, the system was allowed to naturally cool to room temperature, yielding the FeNi@Lig catalyst. The ensuing material underwent multiple cycles of washing with ethanol and DW, centrifugation, and subsequent drying overnight at 60 °C.

The prepared Fe-Ni@Lig catalyst was used for the optimized chemocatalytic oxidation of BB and the catalyzed oxidative transformation of raw cellulose (RC) [26,35,36]. The oxidation of BB pollutants was investigated through an optimization of the process conditions as detailed in Table 2. The Fe-Ni@Lig catalyst (1, 2, and 4 wt%) was added to a mixture of 25 mL of H₂O₂ (2×10^{-4} and 4×10^{-4} M), and 25 mL of BB contaminant with initial concentrations of 10, 50, and 100 mg/L. Subsequently, each concentration-specific mixture underwent stirring at ambient temperature for the designated duration. To gauge and track the advancement of the catalyzed reaction and assess the rate of oxidized bromothymol blue (OBB), UV-Visible spectrophotometry was employed. Furthermore, the optimization of RC catalyzed oxidation was realized as follows: An amount of RC was introduced into a mixture comprising 50 mL of 30 % H₂O₂, at a solid-to-liquid ratio of 1:10 (w/v), along with 5–10 % of the as-prepared Fe-Ni@Lig catalyst. The ensuing reaction was conducted while manipulating both time spans (30, 60, and 90 min) and temperatures (room temperature to 60 °C) (Table 3). Upon completion of the reaction, centrifugation at 10,000 rpm multiple times facilitated the recovery of oxidized cellulose (OC) and the removal of surplus H₂O₂ solution. The acquired OC was thoroughly washed with deionized water until the water's conductivity measured less than 2 µS/cm and the pH was neutral. After this, the OC underwent overnight drying, rendering it amenable for subsequent characterizations. After each catalyzed oxidative reaction, the functionalized Fe-Ni@Lig product was recovered, and its endurance and reusability were evaluated following multiple rinses with deionized water and drying at 80 °C for several hours.

2.3. Analysis and characterizations

The examination of the samples' structural composition was carried out utilizing a Fourier-transform infrared spectrophotometer (JASCO ATR/FTIR 4600 Type A). Spectral data in the FTIR analysis spanned from 4000 to 400 cm⁻¹, with a resolution of 4 cm⁻¹ and an accumulation of 16 scans. X-ray diffraction (XRD) patterns were generated using a BRUKER X-ray diffractometer (D8 ADVANCE), with a scanning rate of 1°/min. Examination of morphological features was conducted with a Zeiss Evo 10 scanning electron microscope (SEM) operating at 15 kV. Prior to SEM analysis, a conductive gold layer was deposited on the sample surfaces using an ion-sputtering system. Elemental composition and distribution in the samples were characterized using an energy-dispersive X-ray analyzer (EDX). The specific surface area and pore size of the samples were assessed through the BET technique, employing a Quantachrome Autosorb instrument (Version 1.27, Boynton Beach, Canada) under N₂ gas adsorption conditions, with gas and bath temperatures maintained at 75 °C and 77.35 °C, respectively.

The thermal stability and degradation behavior of the samples were evaluated through thermogravimetric analysis (TGA) using a LABSYS Evo TGA 1600 instrument from SETARAM Instruments. Each sample (10 mg) was subjected to heating from room temperature to 700 °C at a rate of 10 °C/min under a N₂ atmosphere. Zeta potential measurements were conducted with a Malvern Zetasizer Nano ZS90 potentiometer (Malvern Instruments in Worcestershire, UK) to assess the surface charge of the materials. Absorbance measurements were carried out to monitor the progress of the BB oxidation process using a UV-Visible spectrophotometer (JASCO V-730 model) over a wavelength range of 200 to 800 nm. The determination of rate constants for the catalytic reaction involved tracking changes in peak intensity at wavelengths of 590 nm for BB and OBB, while the catalyst's efficiency was determined by evaluating the conversion rate of BB utilizing Eq. (1), where C₀ and C_t denote the initial and final dye concentrations, respectively [37,38]:

$$\text{Conversion (\%)} = \frac{C_0 - C_t}{C_0} \times 100 \quad (1)$$

The turnover frequency (TOF) was determined for the purpose of evaluating the effectiveness of the catalyst. TOF is defined as the ratio of moles of substrate to moles of active sites in the catalyst per unit time [39,40]. The calculation of TOF was conducted in accordance with Eq. (2), where n(Ox) represents the oxidized material (mol); n(cat) is the quantity of active sites in the catalyst (mol), and t denotes the reaction time (min). TOF was calculated in accordance with Eq. (2), using the ratio of oxidized material to active sites in the catalyst over reaction time. The data presented, including conversion rates, TOF values, and composition percentages, were determined with an experimental error of ±2 %. Retaining two decimal places for conversion rates and TOF values ensures accurate representation of small but meaningful differences in the data. The TOF values and composition percentages were determined with an experimental error of ±2 %. Maintaining two decimal places for conversion rates and TOF values ensures accurate representation of small but significant differences in the data.

$$\text{TOF (min}^{-1}\text{)} = \frac{n(\text{Ox})}{n(\text{cat}) \times t} \quad (2)$$

Utilization of X-ray Photoelectron Spectroscopy (XPS) analysis was implemented to characterize the surfaces of the catalysts and evaluate alterations in samples post-functionalization. The specimens underwent examination utilizing Versaprobe 3 CE (Phi, Chanhassen, US) equipped with a monochromatic Al-Kα X-ray source and configured with PHI Multipak software. The acquired spectra were obtained with the charge neutralizer set at a 200 µm spot size, utilizing 224 eV pass energy with increments of 0.8 eV.

Quantification of hydroxyl compounds in untreated and functionalized lignin/cellulose samples was carried out by simultaneous conductometric titration in aqueous media. This analysis was carried out using a T50 automatic titration unit combined with an InLab 718 conductometric probe (Mettler Toledo, Greifensee, Switzerland). 1 g of the material was introduced into 100 mL of DW, with 10 mL of 1 M NaOH, and the mixture was homogenized for a few minutes until completely dissolved. To lower the pH to 2, a solution of 1 M HCl was progressively added. To prevent the neutralization of NaOH by atmospheric CO₂, the titration vessel was carefully sealed with plastic film. Hydroxyl content was determined using the methodology described in previous studies [31,41]. Each sample was measured three times to ensure accuracy and consistency. Furthermore, the carboxyl rate of OC was assessed by conductometric titration to estimate the degree of oxidation (DO) [29,42]. Briefly, 0.1 g of dried oxidized cellulose was dispersed in 60 mL of water. Before titration, 2.5 mL of 0.1 M HCl was introduced, and the resulting mixture was then titrated using 0.1 M NaOH. The quantification of carboxyl groups was reported in mmol/g.

The assessment of the oxidation rate of oxidized cellulose was performed to determine the extent of oxidation (DO, %). A total of 100 mg of dried oxy-cellulose (OC) was placed into a solution comprising 100 mL of DW and 10 mL of 0.01 M NaCl. The pH level was adjusted to 2.5 through the addition of 0.1 M HCl. Titration was executed utilizing a T50 automatic titration unit, with the addition of 0.05 M NaOH solution at a rate of 0.25 mL/min until reaching a pH of 11. To ensure precision and mitigate impurity influences, a blank titration was carried out without any OC sample to calibrate the system. Conductivity was plotted against the volume of NaOH, and the resulting data was utilized to compute the quantity of oxidized groups. Degree of oxidation (DO) % is expressed as the ratio between the quantity of oxidized hydroxymethyl groups and the total hydroxymethyl groups present [43,44]. The FeNi@Lig materials were utilized in successive catalytic operations under optimal conditions. The recuperation rate of the catalysts was reevaluated employing Eq. (3), in which mr represents the dry mass of reused catalyst (g), and mf signifies the dry mass of fresh catalyst (g):

$$\text{Catalyst recovery (\%)} = \frac{m_r}{m_f} \times 100 \quad (3)$$

3. Results and discussion

3.1. Characterizations of lignin-functionalized bimetallic catalysts

3.1.1. Structural analysis and physicochemical features

Fig. 1a illustrates the plotted FTIR spectrogram of RL and Fe-Ni@Lig catalyst. Before functionalization, RL showed typical characteristic groups of lignin. Specifically, the broadband located around 3295 cm^{-1} is attributable to the significant presence of phenolic and aliphatic OH, while the typical methyl/ethyl groups are characterized by the peak at 2937 cm^{-1} [32,37]. The emergence of the peak observed at 1733 cm^{-1} can be attributed to the presence of the carbonyl group within RL, particularly those related to carboxylic and ketone/aldehyde functionalities [45,46]. The characterization of lignin's aromatic nature is distinguished by the peaks detected at 1587, 1360, 1258, and 1125 cm^{-1} , which are linked to aromatic skeletal vibrations such as C=C, C—C, and C—H bonds [47,48]. The appearance of the peak at 1020 cm^{-1} in RL is associated with the in-plane aromatic C—H stretching of the guaiacyl lignin type [41]. Additionally, the band identified at 835 cm^{-1} corresponds to out-of-plane C—H bonds present in the HGS monomers [45,49]. The FTIR of the Fe-Ni@Lig catalyst markedly exhibits a typical pattern of the carbonized lignin material. The thermochemical treatment reduced the intensity of the OH bands, as well as decreased the bands at 1360, 1258 and 1125 cm^{-1} , suggesting the decline of oxygenated functionalities [50]. Moreover, carbonization promotes the development of a densely branched aromatic structure, resulting in decreased linkages between units and a reduction in C3/C5 methoxyl in the lignin, which in turn encourages the formation of a graphene-like structure [22,51]. Furthermore, the FTIR spectra showed shoulder bands at 450 and 435 cm^{-1} associated with Ni—O and Fe—O stretching [35]. The active sites on lignin, characterized by oxygen-containing groups ready for chemical reactions, play a crucial role in enabling effective surface adsorption and catalytic control. These active sites significantly contribute to enhancing the catalytic capabilities of the material. The spectrogram of Fe-Ni@Lig demonstrates the successful functionalization and deposition of the bimetallic system onto the lignin groups of the catalyst.

XRD patterns of RL and Fe-Ni@Lig are illustrated in Fig. 1b. The samples exhibited distinct variations in their crystallographic properties, primarily attributed to the physicochemical changes brought about by lignin functionalization. In particular, RL displays a characteristic amorphous structure, which arises from the complex and heterogeneous macromolecular composition of lignin. This structure consists of multiple branched subunits featuring various physical and chemical bonds. The broad peak evident at about 22 degrees in the XRD pattern of RL strongly indicates the amorphous nature inherent in lignin [49,52]. However, the Fe-Ni@Lig catalyst showed different crystallographic behavior. The diffractogram peaks of (111), (200) and (220) crystal planes at 45° , 52° and 72° demonstrated the presence of FeNi alloy in the bimetallic catalyst [11,53]. The presence and growth of Fe NPs on the carbonized framework was also revealed by the appearance of different crystallographic plans of iron carbide [54]. The reductive character of lignin indeed can promote the formation of the $\text{Fe}^0\text{-Ni}^0$ system [55]. The crystallinity diffraction pattern of Fe-Ni@Lig showed the successful inclusion of bimetallic catalysts in the lignin biopolymer.

XPS analysis conducted on both untreated and modified lignin-based catalysts is presented in Fig. 1c-h. In the case of untreated lignin, prominent signals from carbon (C) and oxygen (O) elements were detected in the XPS survey spectra. Particularly, the high-resolution XPS analysis of the native lignin separated the C 1 s peak into distinct categories: C—C/C=C (284.3 eV) and carbon species within alcohol or ether groups (286.1 eV) (Fig. 1) [7,55,56]. Furthermore, the deconvolution of the O 1 s spectra for untreated lignin revealed peaks at binding energies

of 521.7 eV and 532.6 eV, corresponding to lattice oxygen (O lattice) and surface hydroxyl groups (—OH), respectively [57–59], as well as separate peaks with the binding energies of 530.9 (C=O), and 535.5 eV (O—C=O) [52]. These functional groups are indicative of the inherent characteristics of lignin, contributing to its diverse and reactive properties, aligning with findings from structural FTIR analysis and other previous studies [55,60,61]. Crucially, a comparison of the XPS spectra between untreated lignin and FeNi@Lig confirms the presence of the FeNi system with alterations in the C 1 s and O 1 s signals. Particularly, the deconvoluted Fe 2p spectra for FeNi@Lig displayed peaks at binding energies of 709.3 eV, 725.4 eV, and 731.5 eV, corresponding to Fe^{2+} , Fe^{3+} , and the satellite peaks of Fe $2p_{1/2}$, respectively [62]. The peaks at 856.5 eV belong to Ni $2p_{3/2}$ and the peak at and 873.1 eV is assigned to Ni $2p_{1/2}$. The satellite peaks are seen at 879.1 eV and 849.8 eV [11,63]. Subtle shifts in the positions and intensities of characteristic lignin peaks are evident post-functionalization. Moreover, the unique peaks associated with iron-nickel within the catalyst validate the successful loading of FeNi nanoparticles onto lignin, potentially enhancing catalytic activity in the relevant transformation process.

3.1.2. Morphological analysis and thermal behavior

The morphologies of RL and FeNi@Lig catalysts were evaluated through SEM analysis, and the corresponding images are displayed in Fig. 2. The RL particles exhibit a spherical or irregular shape, characterized by a rough surface texture that reflects the intrinsic structure of lignin. Lignin is known to be a heterogeneous and amorphous biopolymer containing varied frameworks and functional groups. The particle size distribution also appears to be diverse, underscoring the heterogeneous nature of RL [64,65]. Examination of the SEM images of the FeNi@Lig catalyst shows notable morphological alterations post-functionalization. The catalyst surface displays enhanced structure and definition, demonstrating a porous architecture crucial for catalytic applications. This porosity plays a vital role in increasing the available surface area for chemical reactions [18,66]. Elemental mapping images illustrate the localized distribution of Fe—Ni particles on the lignin surface, with Fe at 2.33 % and Ni at 2.46 %, indicating successful metal incorporation and functionalization within the lignin framework. The combination of the porous structure and surface functional groups of lignin, coupled with the reactivity of the concentrated embedded bimetallic system, offers improved catalytic performance. Moreover, the catalyst's porosity facilitates significant mass transfer, ensuring efficient access of reactants to active sites and leading to favorable catalytic outcomes [67].

Furthermore, the relatively low specific surface area of RL ($0.146 \text{ m}^2/\text{g}$) is indicative of raw lignin possessing a compact and non-porous structure. This limited surface area implies a scarcity of active sites for catalytic reactions or adsorption phenomena in RL. Examination through SEM reveals a notable augmentation in specific surface area post functionalization, increasing from $0.146 \text{ m}^2/\text{g}$ for RL to $99.79 \text{ m}^2/\text{g}$ after partial carbonization and introduction of Fe—Ni, indicating a substantial modification in the material's architecture. Carbonization can induce the generation of a more porous structure by eliminating volatile components and promoting thermal decomposition [68,69]. The presence of Fe and Ni is likely to play a role in this transformation by serving as catalysts that expedite the development of a porous carbon framework. Enhanced surface area post-functionalization indicates a potential elevation in catalytic performance [66]. The hydroxyl of lignin is of crucial importance, as it is considered one of the main functional characteristics of this biopolymer, and the responsible for its behavior and performance [7,70]. In its raw state, lignin exhibits an OH rate of approximately 3.98 mmol/g. However, through functionalization processes, this value undergoes a substantial reduction to 0.46 mmol/g. The decline in hydroxyl content post-functionalization can be attributed to the incorporation of metals and the application of carbonization treatments. The introduction of metals during functionalization processes alters the chemical composition of lignin, leading to a modification of its

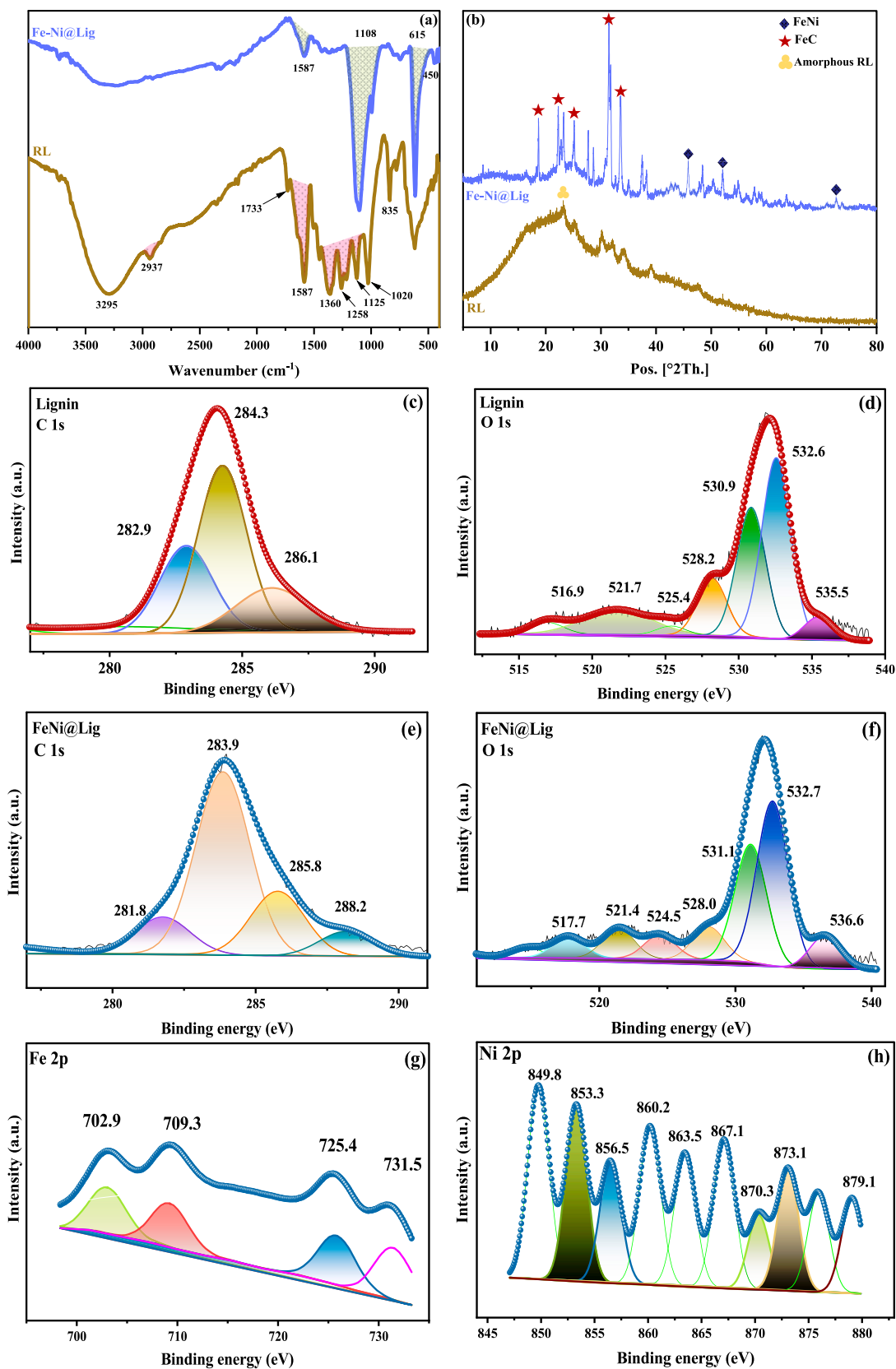


Fig. 1. (a) FTIR and (b) XRD analysis of raw lignin (RL) and FeNi@Lig catalysts. (c-h) XPS of unmodified lignin and FeNi@Lig catalyst: Deconvoluted XPS spectra of C 1 s, O 1 s and Fe/Ni systems for raw and functionalized lignin.

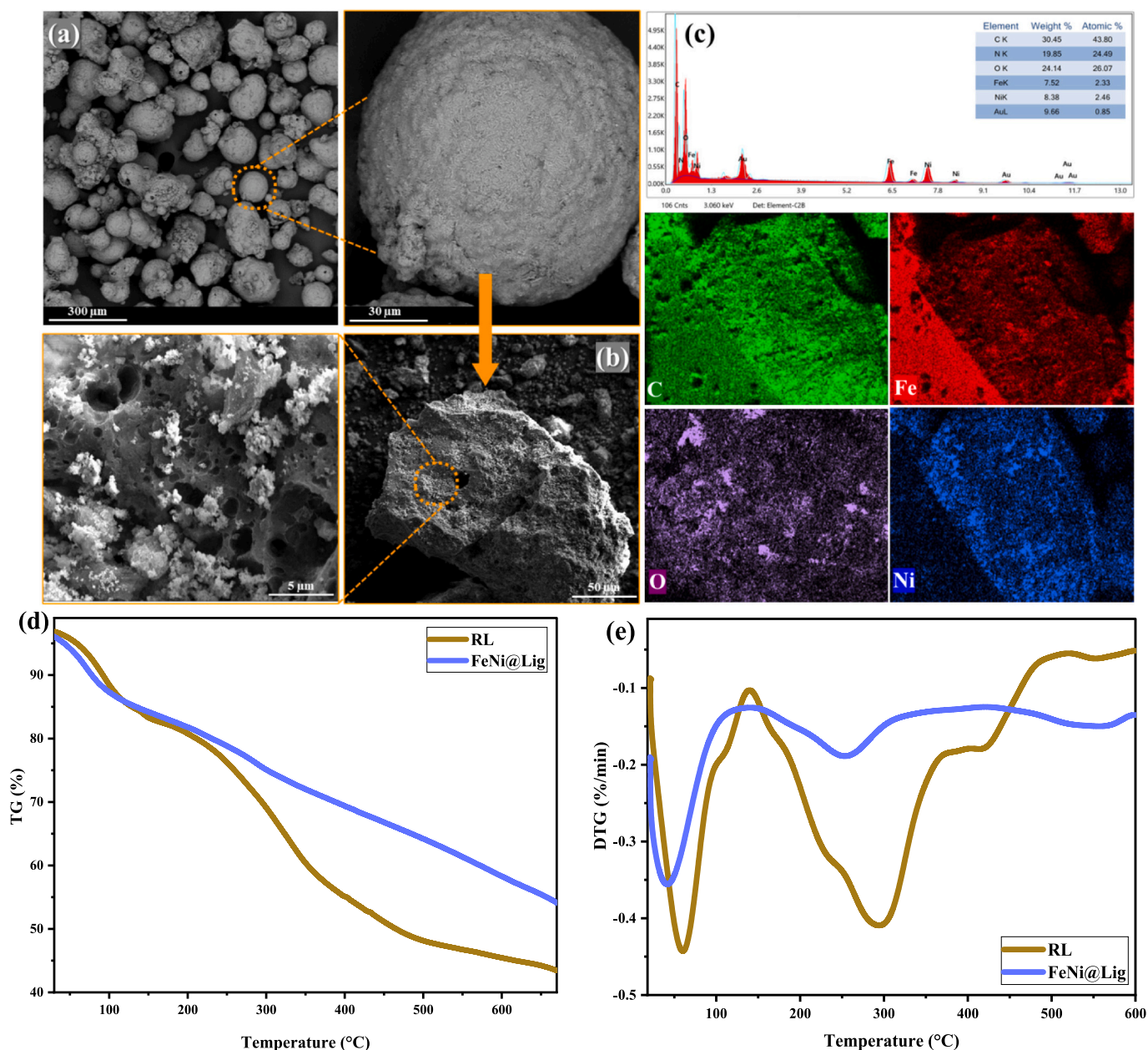


Fig. 2. SEM images of RL (a) and FeNi@Lig (b), and the corresponding catalyst elements EDX mapping analysis (c). (d) TGA and (e) DTG of RL and FeNi@Lig catalyst.

functional groups, particularly OH. Additionally, carbonization treatments contribute to this reduction by inducing structural changes in lignin, resulting in a notable decrease in the number of hydroxyl groups available [16,71]. The zeta potential of the FeNi@Lig catalyst measured at -22.7 mV is markedly lower than that of untreated lignin (-15.5 mV)

(Table 1). Importantly, these values signify the remarkable stability of dispersed catalytic functional nanoparticles and a notable reduction in aggregation phenomena [39,55,72]. The porous morphology of functionalized lignin plays a significant role in enhancing catalytic efficacy that transcends the mere augmentation of surface area. It facilitates mass

Table 1

Surface properties and elemental analysis of functionalized bimetallic catalysts and oxidized materials.

Sample	COOH (mmol/g)	S_{BET} (m^2/g)	Zeta potential (mV)	Elements level (%)			
				C	O	Fe	Ni
Raw lignin (RL)		0.146	-15.5	40.24	43.80		
Fe-Ni@Lig		99.79	-22.7	43.80	26.07	2.33	2.46
Raw cellulose (RC)			-11.6	60.94	31.12		
Oxy-cellulose (OC)	1.96		-24.4	68.88	37.40		
Reused Fe-Ni@Lig (OBB)			-20.3				
Reused Fe-Ni@Lig (OC)			-17.8				

transfer by establishing pathways for the effective diffusion of reactants and products, thereby diminishing diffusion resistance during catalytic processes. This characteristic is especially beneficial for oxidative reactions, in which the swift transport of reactants and expeditious removal of intermediates are imperative [5,73,74]. Furthermore, the porous configuration fosters the homogenous distribution of FeNi nanoparticles, thereby reducing agglomeration and ensuring consistent availability of active sites. The chemical functionalities present within the pores, such as hydroxyl and carbonyl moieties, additionally promote electron transfer and substrate interaction, thereby enhancing catalytic turnover efficiency [5,17,75].

The presentation of TGA and DTG data for the RL and FeNi@Lig catalyst is depicted in Fig. 2c, d. The thermal profiles of both untreated and modified lignin indicate distinct thermal behaviors characterized by multiple degradation steps. Particularly, unaltered raw lignin displays typical lignin traits, manifesting initial weight loss below 140 °C, indicative of volatile release and moisture evaporation [45,76]. Subsequently, the materials undergo the main degradation phase within the range of 140–370 °C for RL and approximately 140–380 °C for FeNi@Lig. This phase involves de-hydroxylation and cleavage of polyphenolic compounds and ether (C–O–C) linkages within the lignin structure [45,77]. Continuous weight loss throughout the temperature escalation stage for both specimens signifies the degradation of macromolecules, the disruption of lignin aromatic structures, the elimination of OCH₃ groups, and the degradation of oxygen-containing functional groups [7,68,69]. The DTG peak for RL is observed at approximately 295 °C, while for the FeNi@Lig catalyst, it is detected at 260 °C. Alterations in thermal behavior are induced by the specific treatments applied, in which the inserted metals can catalyze the graphitization process, which increases the thermal resistance of the FeNi@Lig catalysts. The thermal properties of Lig-Co NPs catalyst demonstrate significant conformity with the documented efficiencies of different supported catalytic systems [78,79]. Remarkably, the FeNi@Lig catalysts demonstrate thermal stability and satisfactory thermal performance, indicating their potential suitability for intended operational conditions. The overall physicochemical properties of FeNi@Lig are in line with previously reported functionalized bi-metal catalysts [11,34,80]. The implementation of lignin as a support and bio binder for immobilization plays a vital role in utilizing its inherent abundance and sustainability. Furthermore, it contributes to the reinforcement of structural robustness and the enhancement of the functionalization potential of the catalyst.

3.2. Performance of lignin-functionalized bimetallic Fe–Ni catalyst

3.2.1. Oxidation of bromothymol blue

The catalytic performance of the prepared bimetallic system (Fe-Ni@Lig) was initially assessed by conducting a series of experiments to examine its effectiveness as a catalyst. This evaluation focused on the catalyzed oxidation of BB, a compound known for its harmful characteristics and environmental impact [26,81]. The remediation of such hazardous organic contaminants holds immense significance due to the challenging nature of these compounds. These contaminants typically feature structurally robust and intricate aromatic systems that are resistant to natural biodegradation processes. Consequently, addressing their removal necessitates the utilization of dependable and efficient oxidation treatment methods [27,36]. Various sets of reaction conditions were employed to assess how the catalytic activity of the Fe-Ni@Lig catalyst impacts pollutant removal. The tests aimed to identify and optimize the key response parameters for environmental remediation, particularly when employing bio-based heterogeneous catalysts. The results are depicted in Table 2 and Fig. 3. The BB catalytic oxidation process was closely monitored by continuous recording of UV–Vis absorption spectra at different time intervals. This enabled the evaluation of the degradation profile catalyzed by the Fe-Ni@Lig. Specifically, changes in peak intensity at a wavelength of 590 nm were examined as a

Table 2
Conversion rates for OBB optimization over Fe-Ni@Lig catalyst.

Run	[H ₂ O ₂] 10 ⁻⁴ .M	[BB] mg/L	Catalyst %	Conversion %
1	2	10	1	97.81
2	2	10	2	97.62
3	2	10	4	94.54
4	2	50	1	98.11
5	2	50	2	99.08
6	2	50	4	96.16
7	2	100	1	93.65
8	2	100	2	96.44
9	2	100	4	98.13
10	4	10	1	96.15
11	4	10	2	98.75
12	4	10	4	97.14
13	4	50	1	95.68
14	4	50	2	96.13
15	4	50	4	91.17
16	4	100	1	99.35
17	4	100	2	98.24
18	4	100	4	96.82
19	2	50	0	19.64
20	4	100	0	15.86

key indicator of the transformation occurring during catalytic oxidation.

Fig. 3a–b shows the optimal UV–Vis output for OBB at [H₂O₂] = 2 × 10⁻⁴ M with [BB] = 50 mg/L, and 4 × 10⁻⁴ M for with [BB] = 100 mg/L. As the reaction time extended for all tested concentrations, there was a clear reduction in the intensity of the characteristic peaks of BB. This decline in peak intensities was empirically corroborated by a visible change in color, transitioning from blue to colorless. Interestingly, the concentration of hydrogen peroxide is a crucial factor in the catalytic oxidation process. Higher concentrations of H₂O₂ typically provide more oxidizing power, as it is a strong oxidizer that can enhance oxidation [28,44]. In general, increasing the concentration of H₂O₂ leads to higher conversion percentages. This is evident in Table 2, where for each given set of [BB] and catalyst percentage, higher [H₂O₂] values are associated with higher conversion percentages. Moreover, a higher initial BB concentration often results in lower conversion percentages, as more BB molecules must be converted. As seen in Table 2, in most cases, higher [BB] levels lead to lower conversion rates. On the other hand, the percentage of Fe-Ni@Lig catalyst plays an essential role in the catalytic oxidation process. It determines the amount of catalyst available to facilitate the reaction. Increased catalyst levels generally lead to improved conversion efficiency. For constant [H₂O₂] and [BB], increasing the catalyst percentage tends to result in higher conversion percents. Interestingly, uncatalyzed reactions under optimal conditions revealed significantly low transformation (15.86 %), demonstrating the catalyst's effectiveness in degrading BB dyes.

Meanwhile, there are some interactions between the parameters that affect the conversion of BB. For instance, when [H₂O₂] is high, a higher [BB] concentration may lead to reduced conversion percentages, indicating that the effect of [BB] could outweigh the effect of [H₂O₂] in certain cases. However, with higher catalyst percentages, the negative effect of higher [BB] can be mitigated. Correspondingly, the most favorable BB conversion rate of 99.35 % was attained within a 3-min timeframe with the conditions of [H₂O₂] at 4 × 10⁻⁴ M, [BB] at 50 mg/L, and a 2 % catalyst concentration. In a parallel manner, a 99.08 % conversion rate was achieved within 4 min using [H₂O₂] at 2 × 10⁻⁴ M, [BB] at 100 mg/L, and a 1 % catalyst concentration. Importantly, in the absence of a catalyst, the reaction was not completed even after 32 min, with the conversion rate remaining at 53 %. The efficiency of the oxidation potential of Fe-Ni@Lig at higher concentrations involving these deleterious compounds is intriguing. This underlines the reliability and effectiveness of bio-based catalysts in the context of environmental pollution control.

Investigating the reaction kinetics enables a deeper understanding of the catalytic performance of the bimetallic lignin-based catalysts. It also

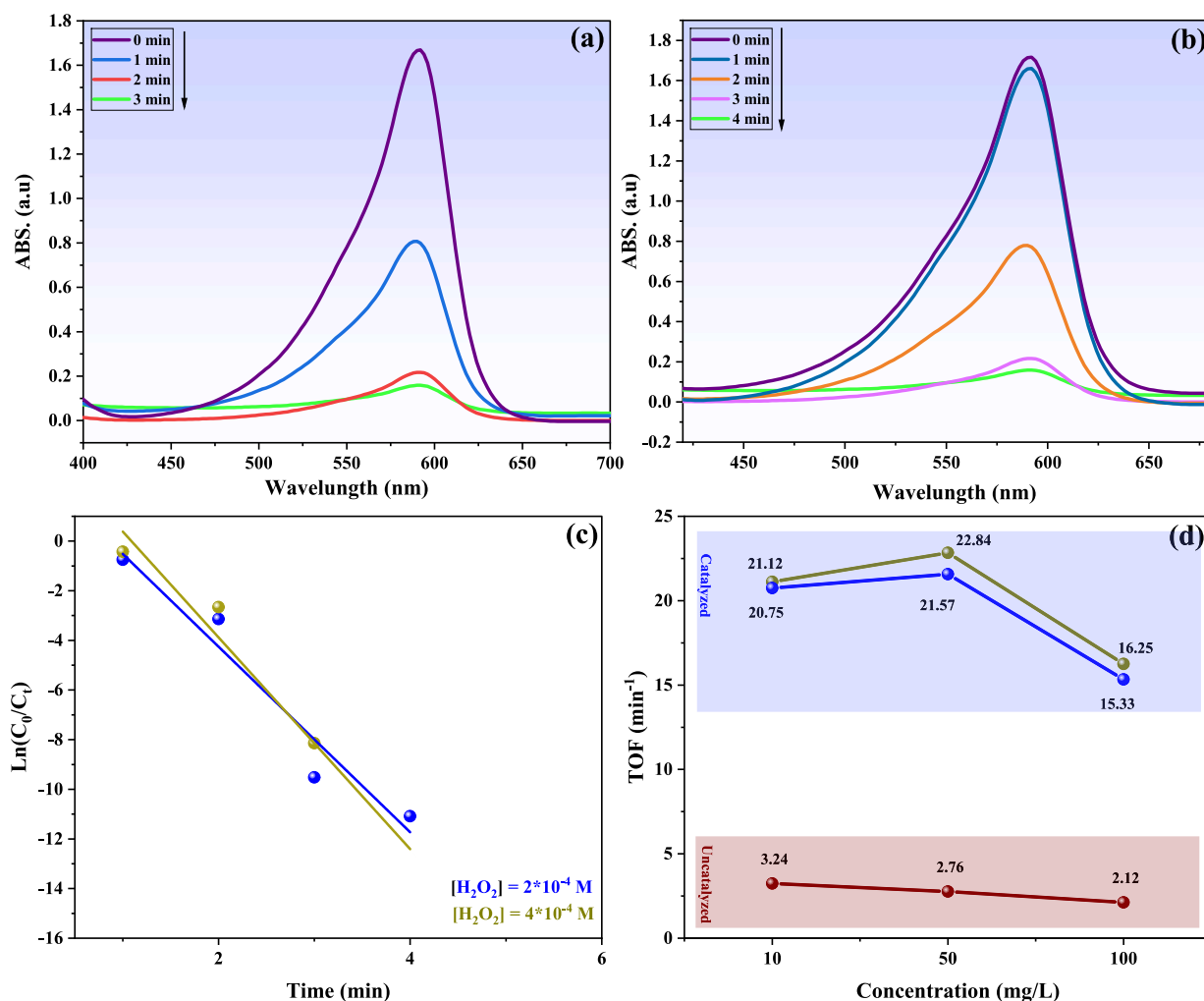


Fig. 3. Changes in the UV-Vis spectra of OBB as a function of time via the Fe-Ni@Lig catalytic reaction: Optimum conversion at $[\text{H}_2\text{O}_2] = 4 \times 10^{-4} \text{ M}$ (a) and $[\text{H}_2\text{O}_2] = 2 \times 10^{-4} \text{ M}$ (b). Correlating plots of $\ln(C_t/C_0)$ as a function of degradation time of BB (c). TOF of catalytic oxidation of BB over Fe-Ni@Lig catalyst (d).

Table 3

Optimization of cellulose oxidation over Fe-Ni@Lig catalyst.

Run	Time min	Temperature °C	Catalyst %	DO (%)
1	30	25	5	48.74
2	30	25	10	69.45
3	60	25	5	66.42
4	60	25	10	71.98
5	90	25	5	80.69
6	90	25	10	82.55
7	90	60	5	89.31
8	90	60	10	83.79
9	30	60	5	76.84
10	30	60	10	79.12
11	60	60	5	91.11
12	60	60	10	85.66
13	60	60	0	27.11

makes it possible to assess the influence of different reaction conditions on the rate of the process and to estimate the activation energy for oxidation [16,27]. The plot of $\ln(C_t/C_0)$ versus time is illustrated in Fig. 3c. Notable linearity is obtained with the variation of time for both used $[\text{H}_2\text{O}_2]$ concentrations. This linear coherence reflects the alignment between model design and real test outcomes. The reaction rate constant k was determined by analyzing the slopes of the linear relationships. The optimized values of k were found to be 0.1532 s^{-1} at 3 min for $[\text{H}_2\text{O}_2] = 4 \times 10^{-4} \text{ M}$, and 0.1721 s^{-1} and $[\text{H}_2\text{O}_2] = 2 \times 10^{-4} \text{ M}$.

The presence of the oxidizing agent appears to enhance the reaction up to a certain point, influencing the overall transfer rate. Nevertheless, the catalyzed reaction achieved a desirable and highly efficient rate for the rapid transformation of BB molecules (3–4 min). Fig. 3d illustrates the TOF of the Fe-Ni@Lig catalyzed BB oxidation. Notably, the estimated optimal TOF values were 21.12 min^{-1} , 22.84 min^{-1} , and 16.25 min^{-1} for [BB] of 10, 50, and 100 mg/L, respectively. These values significantly surpass the uncatalyzed transformations (3.24 min^{-1}), underscoring the significance and efficacy of the catalytic approach involving a functionalized lignin-bimetallic system. The catalytic behavior is ultimately attributed to the lignin functionality and the promotion capacity of the FeNi system.

3.2.2. Oxidation of cellulose over Fe-Ni@Lig catalyst

Cellulose and its derivatives represent a class of non-toxic, biodegradable polysaccharides widely acknowledged as one of the safest and most versatile polymer groups. They find extensive applications in diverse sectors such as textiles, food, composites, wastewater treatment, medical products, and hold promising potential in bio-energy production [82,83]. Oxidation stands out as a particularly auspicious process for introducing new functional groups to cellulose, a method frequently employed to either imbue specific properties or modify existing ones. This transformative process allows for the precisely controlled conversion of cellulose into intermediary compounds or platform chemicals, serving as invaluable precursors for the synthesis of a broad spectrum of

bio-based materials and chemicals [29,43]. The oxidized cellulose was prepared using a FeNi@Lig catalyst under optimized conditions, as detailed elsewhere. Specifically, raw cellulose was reacted with 30 % hydrogen peroxide at a solid-to-liquid ratio of 1:10 (w/v) and a catalyst loading of 5–10 % (w/w) at temperatures ranging from 25 to 60 °C for varying reaction times (30–90 min).

Fig. 4 presents the structural and compositional changes observed in oxidized cellulose compared to raw cellulose. In the FTIR spectra of non-oxidized cellulose (Fig. 4a), the raw cellulose (RC) exhibited characteristic OH bands at around 3336 cm^{-1} , along with vibration of C—H and CH_2 at 2890 cm^{-1} [84,85]. The peak at 1636 cm^{-1} was attributed to hydrogen bonding in OH stretching and bending vibrations of water [86]. Additionally, the peaks at 1430 cm^{-1} , 1366 cm^{-1} , and 1315 cm^{-1} were assigned to CH, C—O, and C—H bending, respectively [84,87]. Moreover, bands within the range of 1100 cm^{-1} to 895 cm^{-1} indicated the existence of β -glucosidic ether linkages of anhydro-glucopyranose ring skeleton, and to the β -glycosidic linkages between the anhydro-glucose units in the cellulose [85,88]. Interestingly, the spectra of the oxidized cellulose (OC) revealed the appearance of an intense band at 1730 cm^{-1} , assigned to the C=O of carboxyl groups [29,43,82]. This observation strongly suggests the successful conversion of unmodified cellulose into oxy-cellulose through the mediated FeNi@Lig catalytic transformation, indicating the introduction of carboxyl functional groups. Moreover, XRD analysis was employed to assess crystallinity before and after cellulose transformation. As seen in Fig. 4b, XRD analysis revealed that oxidized cellulose (OC) exhibited a spectrum resembling that of original raw cellulose (RC), indicating that the crystalline structure had not been altered during the oxidation process. Notably, both RC and OC materials showed peaks characteristic of crystalline cellulose I, including a strong peak at $2\theta = 22.5^\circ$ and three less defined peaks at $2\theta = 14.8^\circ$, 16.2° and 34.4° , which correspond to the typical crystallographic planes of cellulose I, namely (200), (110), (110) and (004), respectively [30,89,90]. The crystallinity index (CrI) of RC was measured at 89.03 %, and it showed a slight improvement for OC, reaching 92.10 %. This observation is in line with similar results in the literature concerning the preservation of oxy-cellulose structure after oxidative transformation [29,44]. In sum, apart from the introduction of carboxyl groups (COOH), the oxidation treatment applied had no major impact on the cellulose skeleton. This treatment proved effective and selective, preserving the main features of cellulose without altering its polymorphism, underlining its potential for the controlled modification of cellulose with minimal structural disruption of main cellulose properties and with no change of the polymorphism.

The zeta potential of the RC was -11.6 mV, whereas for OC, it notably decreased to -24.4 mV. The observed decrease in zeta potential between raw and oxidized cellulose indicates a marked alteration in surface charge characteristics. Negative zeta potential values indicate the presence of anionic groups introduced during the oxidation process. In particular, the introduction of carboxylates and oxygen-containing functional groups to the cellulose surface leads to a more negative charge state. In the absence of catalysts, the DO level was measured at 27.11 %. However, the incorporation of 5 % FeNi@Lig catalysts significantly raised this yield, reaching an optimum level of 91.11 %. This significant increase in DO can be attributed to the oxidation of a substantial proportion of the hydroxymethyl groups to carboxyl groups. Optimum TOF results align with these findings, showing a maximum TOF of 38.16 % during catalyzed oxidation. The measured OH rate confirmed these results, in which the extent declined from 3.84 mmol/g to 1.14 mmol/g, due to the catalytic conversion of OH into COOH (Table 1). These results underline the robust catalytic efficiency of lignin-based catalysts in oxidative transformations. The superior performance of this catalyst is attributed to the efficient and stable loading of iron-nickel, the functional structure of lignin and the synergistic effects between catalysts and substrate [39,52]. The thermal stability and degradation behavior of the RC and OC samples were investigated using TGA and DTG. The TGA curves, presented in Fig. 4c, d, illustrate the

weight loss profiles of the samples as a function of temperature. Both the RC and OC samples exhibited a similar overall trend, with a gradual weight loss at lower temperatures followed by a more rapid weight loss at higher temperatures, indicative of the thermal decomposition processes. An initial weight loss was observed below 100 °C, which can be attributed to the evaporation of adsorbed moisture or volatile compounds present in the cellulose structure [84,91,92]. The major weight loss occurred in the temperature range of approximately 300–400 °C with DTG peaks at 335 °C of RC and at 338 °C of OC, corresponding to the thermal decomposition and depolymerization of the cellulose chains [93,94]. A notable shift was observed for the OC sample, suggesting that the oxidation treatment may have altered the thermal decomposition of the oxidized cellulose chains by introducing structural modifications. The observed differences in the TGA and DTG curves between the RC and OC samples indicate that the oxidation treatment has altered the thermal stability and degradation kinetics of the cellulose.

The chemical composition at the surface and the oxidation states of both the RC and OC samples were examined through XPS analysis. Detailed scans of the core levels of C 1 s and O 1 s were conducted to provide insights into the chemical surroundings and oxidation states of these elements. In the case of the RC sample, the C 1 s spectrum (Fig. 4e) displayed three distinct peaks at binding energies of roughly 282.2 eV, 283.8 eV, and 285.4 eV, corresponding to C—C/C—H, C—O, and O—C—O/C=O bonds, respectively. These peaks are indicative of the cellulose structure, with the C—O and O—C—O/C=O peaks representing the oxygenated functional groups inherently present in cellulose [44,95]. Conversely, the C 1 s spectrum of the OC (Fig. 4g) exhibited a more dominant peak at approximately 287.4 eV, attributed to the emergence of new carbonyl (C=O) groups resulting from the oxidation process. Moreover, changes in the relative intensities of the peaks suggest alterations in the chemical environment of carbon atoms due to the incorporation of these newly oxidized functional groups. The O 1 s spectrum of the RC sample (Fig. 4f) revealed a broad peak centered around 532.2 eV, which could be deconvoluted into various components representing different oxygen species found in cellulose, such as C—O, O—C—O, and adsorbed water or hydroxyl groups [96,97]. Interestingly, the O 1 s spectrum of the OC sample (Fig. 4h) displayed a more distinct shoulder or additional peak at approximately 530.3 eV, attributed to the carbonyl (C=O) groups generated during the oxidation process. The heightened intensity of this peak in the OC sample provides further evidence of the successful introduction of new carbonyl functionalities on the cellulose surface because of the oxidation treatment. Additionally, these findings align with the structural analysis conducted through FTIR and XRD techniques on the OC sample.

Overall, the notable catalytic efficacy exhibited by the FeNi@Lig catalyst can be ascribed to the synergistic interplay between Fe and Ni. Iron imparts redox capabilities through its reversible $\text{Fe}^{2+}/\text{Fe}^{3+}$ cycle, whereas nickel serves to stabilize the electronic milieu, thereby ensuring persistent catalytic performance. This interplay effectively optimizes the adsorption and desorption dynamics of reaction intermediates, as iron enhances the binding of oxygen species while nickel promotes the desorption of products. Furthermore, the alloying of iron and nickel alters the electronic architecture, leading to a reduction in the activation energy required for pivotal reaction stages. The structural function of nickel in averting the agglomeration of iron nanoparticles further bolsters the longevity of catalytic activity. These synergistic phenomena culminate in the exceptional conversion rates observed for the oxidation of bromothymol blue and cellulose under mild reaction conditions [98–100].

3.3. Stability and regeneration potential

A proficient catalyst must exhibit a combination of high reactivity and stability, in addition to the capacity for separation and reusability in heterogeneous systems [101–103]. Heterogeneous catalysts provide beneficial potential for regeneration, thus facilitating the use of lignin

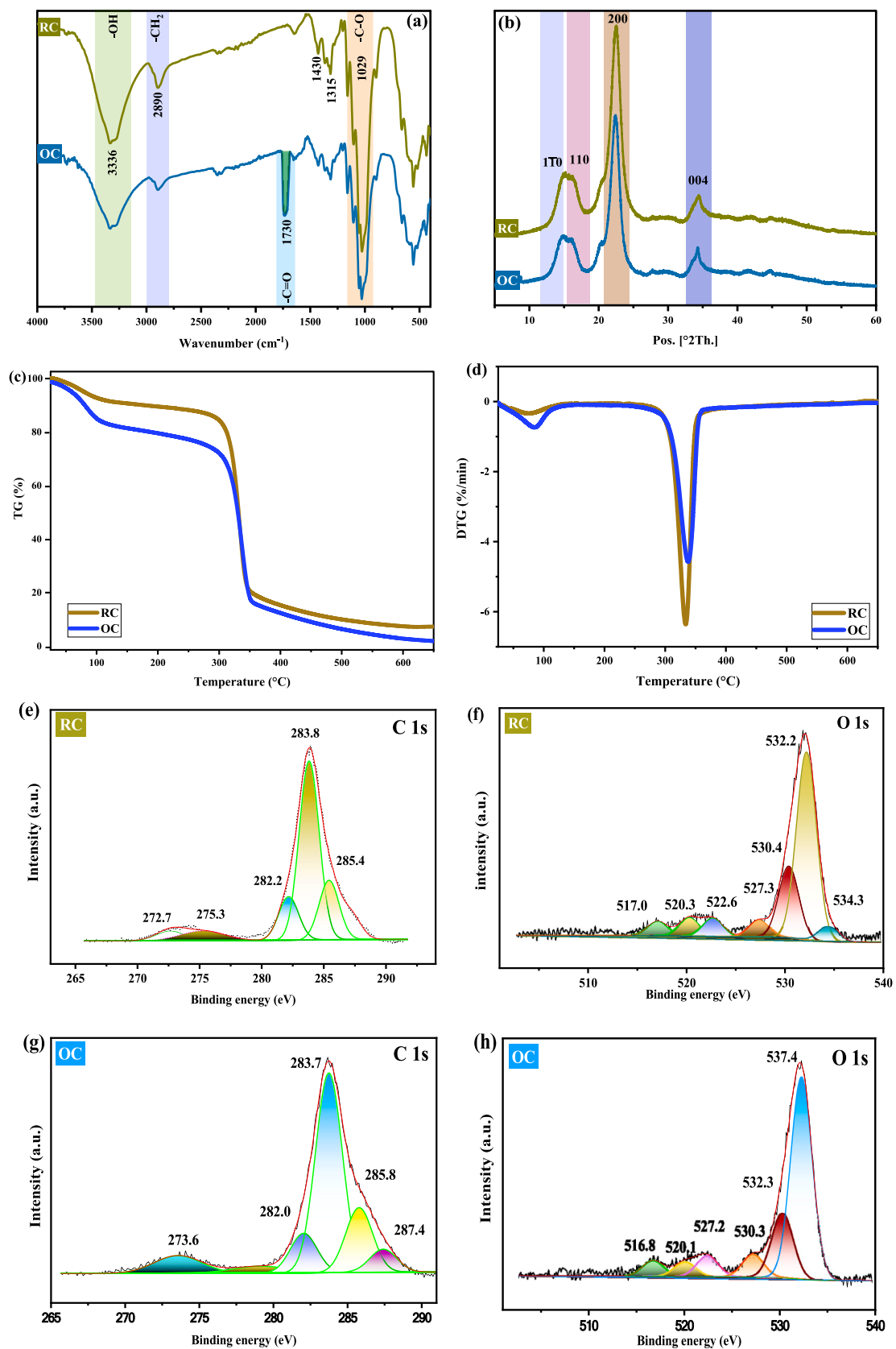


Fig. 4. (a) FTIR and (b) XRD of raw cellulose (RC) and oxidized cellulose (OC) (c, d) TGA/DTG of RC and OC. (e-h) Deconvoluted XPS spectra of RC and OC.

derivatives in diverse chemical transformations [6,7]. The catalytic oxidation process was conducted through multiple cycles under optimal conditions to investigate the reusability and robustness of the FeNi@Lig catalysts. The stability and deactivation of the catalysts were evaluated through the analysis of FTIR and SEM data, as well as the determination of the recovery rate of FeNi@Lig catalyst.

Fig. 5a illustrates the evolution of the catalyst's structure upon reaching the maximum cycle number in the catalyzed oxidation process. It is noteworthy that the spectra of newly reused catalysts showed no significant changes in the catalyst's structure, indicating the presence of characteristic bands of OH at 2937 cm^{-1} and at 1733 cm^{-1} associated with the carbonyl group [45,46]. The involvement of the catalyst in the reaction evidently influences both the physical structure of the catalyst and its chemical bonds [103,104]. As the final cycle progresses, the catalytic active sites become occupied, potentially resulting in a decline in catalytic efficiency for both OBB and OC conversions. The presence of BB or cellulose molecules within the reused catalysts indicates the deactivation of catalytic sites following the recycling assessments. Indeed, the accumulation of organic by-products or reactants on the catalyst surface, which could block active sites and hinder reactant

access [17,103,105]. This fouling effect likely contributes to the reduced catalyst efficiency observed in subsequent cycles for both reactions.

Fig. 5b illustrates the morphology of a fresh catalyst, while Fig. 5c and d demonstrate the alterations over recycling for OBB and OC, respectively. The surface of the unused catalyst appears relatively smooth with porous characteristics, which are essential for catalytic reactions. However, after undergoing oxidation reactions, the surface morphology becomes more aggregated and less distinct compared to its unused state, displaying increased roughness and the presence of larger aggregates. SEM images reveal increased surface roughness and aggregation of active sites, suggesting partial structural degradation.

The replicability of oxidation using lignin-based catalysts may underscore the reproducibility efficacy of these novel bio-derived catalysts. The reuse efficiency of the FeNi@Lig catalyst is delineated in Fig. 5d, e. The conversion efficiencies exhibit a decline with each consecutive cycle, indicating a deterioration in catalytic efficiency over time. The initial three cycles of OBB did not show any significant decrease in activity; however, in the final run, the removal efficiency decreased from 99.35 % to 23.41 %. This implies that the catalyst's effectiveness diminishes after repeated utilization, possibly due to alterations in the

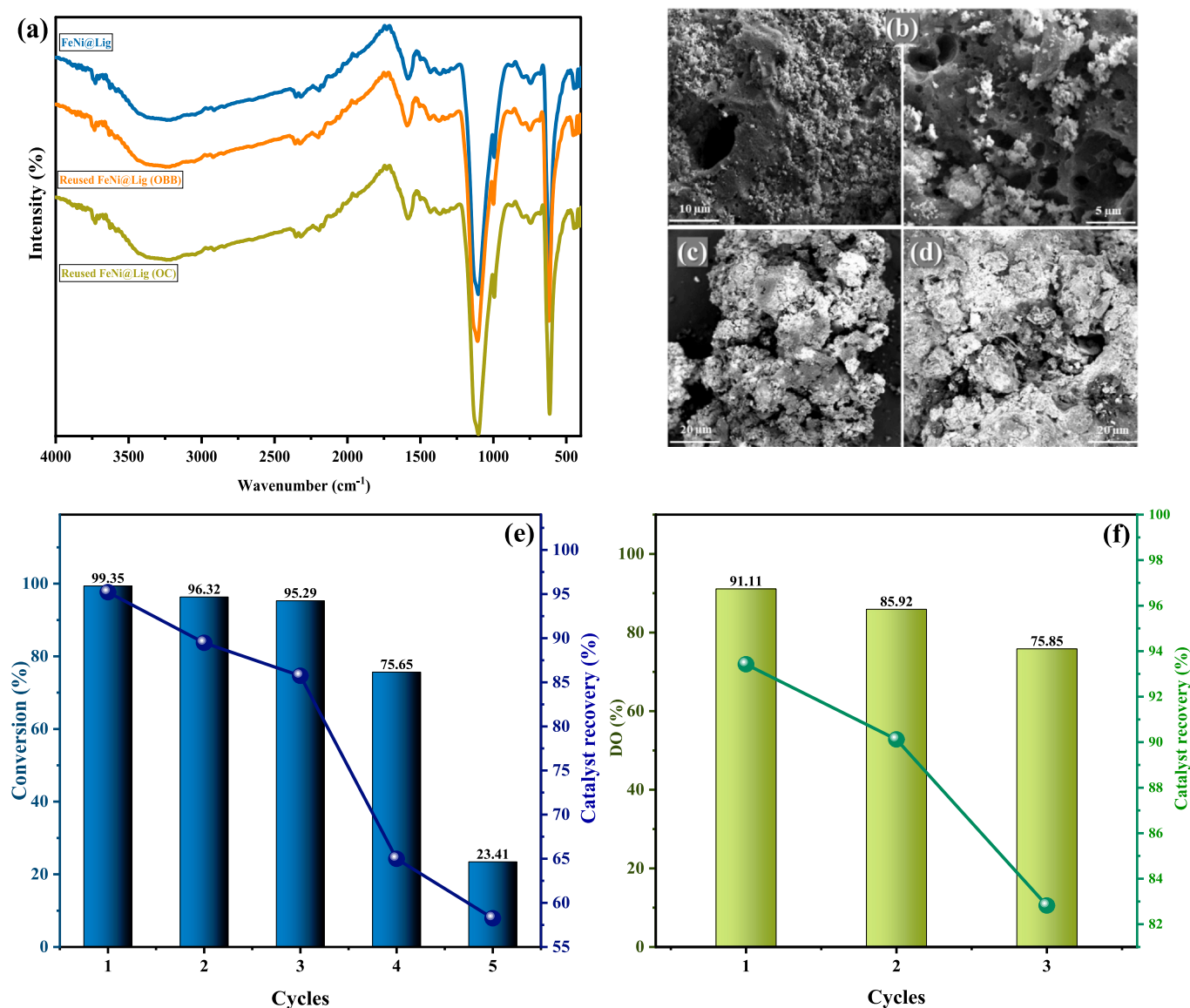


Fig. 5. Reusability of Fe-Ni@Lig catalysts for OBB and OC: FTIR (a). SEM of (b) unused catalyst, (c) reused for OBB and (d) for OC preparation. Recycling of the catalyst for (e) OBB and (f) OC with estimated recovery rate.

structure or deactivation of active sites [68,71]. This was paralleled by a notable reduction in the catalyst's recovery yield from 95.21 % to 58.25 %. A similar pattern was also observed in cellulose oxidation, with a consistent decrease in the catalyst's recovery yield over three cycles. These patterns underscore the difficulty in preserving the stability and efficacy of catalysts across multiple applications. The diminishing performance could be ascribed to potential structural deterioration, fouling of active sites, or loss of active material during the recovery phase.

The oxidative environment of the reaction medium can significantly influence the progressive oxidation of the catalyst surface. Such alterations indicate the emergence of less reactive oxides over time, thereby further diminishing the catalyst's efficacy. The phenomenon of metal leaching is particularly intensified under alkaline or oxidative conditions, which may compromise the interaction between the metal nanoparticles and the lignin substrate [5,22]. This diminution of active sites exerts a direct influence on the overall catalytic activity and selectivity. Throughout the catalytic mechanism, organic by-products or reactants may adhere to the catalyst surface, resulting in the fouling of the active sites. These residues obstruct the accessibility of reactants to the active sites, thereby impairing the performance of the catalyst [106,107]. This fouling phenomenon is notably accentuated in reactions that involve complex substrates, wherein multiple oxidation intermediates are produced. Furthermore, the thermal stress and extended exposure to reactive species may instigate microstructural alterations, such as the agglomeration of metal nanoparticles, consequently diminishing their dispersion and catalytic activity [108,109].

To enhance the practical utility of FeNi@Lig catalysts, a variety of strategies may be implemented. Enhancing the functionalization of the lignin matrix through the incorporation of functional groups such as nitrogen or sulfur can fortify metal-lignin interactions, thereby diminishing metal leaching and improving the stability of active sites [5,22]. The application of protective coatings, including thin layers of carbon or polymers, can avert oxidative degradation and nanoparticle agglomeration, thus ensuring sustained performance over time. The optimization of reaction conditions by alleviating extreme environments, such as excessive pH levels or elevated temperatures, can reduce the risk of structural degradation. The formulation of effective regeneration protocols, such as solvent washing or regulated thermal treatments, can rejuvenate catalytic activity by eliminating fouling residues. Furthermore, the design of composites that integrate stabilizing materials like metal oxides or graphene can furnish both mechanical and chemical support, thereby prolonging the lifespan of the catalyst. Collectively, these strategies confront existing limitations and facilitate the broader industrial integration of lignin-based catalysts in sustainable methodologies.

4. Conclusions

This study highlights the development of Fe–Ni bimetallic functionalized lignin (FeNi@Lig) catalysts, showcasing the synergistic activity of Fe and Ni integrated onto lignin extracted from spent coffee grounds. The use of SCG as a biomass source not only promotes sustainable waste valorization but also introduces a novel, cost-effective material with tailored catalytic properties. The successful completion of this work focused on optimizing the catalytic activity of Fe–Ni bimetallic functionalized lignin for cellulose and BB dye oxidation. The primary investigations emphasize the remarkable catalytic efficiency of these environmentally friendly catalysts in controlling pollution and their potential for transforming cellulose into high-value molecules and chemicals. The physicochemical analysis of the FeNi metal-infused lignin system using techniques like XPS, FTIR, XRD, and SEM demonstrated the effective integration of FeNi metals into the lignin structure. The experimental outcomes significantly validated that the Fe–Ni@Lig catalyst greatly improves the oxidation process, achieving high conversion rates for both BB and cellulose. The optimal conditions for BB oxidation were determined to be $[H_2O_2] = 4 \times 10^{-4}$ M and 2 % catalyst

concentration, leading to a 99.35 % conversion rate within only 3 min. Similarly, cellulose oxidation was optimized, resulting in a degree of oxidation of 91.11 % at 60 min, 60 °C, and 5 % catalyst concentration. The research also emphasized the recyclability of Fe–Ni@Lig catalysts, which maintained superior catalytic efficiency through numerous cycles for both transformative reactions. This reusability highlights the economic and environmental advantages of these natural derived catalysts.

While the FeNi@Lig catalyst exhibits commendable recyclability, the discerned diminution in efficacy after several cycles is ascribed to structural deterioration, metal leaching, and the fouling of active sites. Mitigating these challenges will necessitate the optimization of the functionalization process to augment stability and the formulation of regeneration protocols aimed at reinstating catalytic activity between cycles. Overall, this investigation illustrates the practicality and efficacy of employing Fe–Ni bimetallic functionalized lignin as a catalyst in oxidation processes. The high conversion rates and reusability of the catalysts offer a promising pathway for sustainable industrial applications, particularly in environmental cleanup and the synthesis of valuable chemicals from biomass. However, further extensive efforts are necessary to exploit the optimized strategies for integrating biomass resources sustainably into catalytic reactions on a large scale.

CRedit authorship contribution statement

Mehdi Mennani: Writing – original draft, Methodology, Investigation, Formal analysis, Data curation, Conceptualization. **Youness Abdellaoui:** Writing – original draft, Methodology, Formal analysis, Data curation. **Anass Ait Benhamou:** Writing – review & editing, Resources, Formal analysis, Conceptualization. **Eduardo Alberto Lopez-Maldonado:** Software, Formal analysis. **Meriem Kasbaji:** Writing – original draft, Investigation, Formal analysis. **Mounir El Achaby:** Writing – review & editing, Visualization, Supervision. **Amine Moubarik:** Writing – review & editing, Visualization, Validation, Supervision. **Zineb Kassab:** Writing – review & editing, Visualization, Validation, Supervision.

Declaration of competing interest

The authors declare that they have no known competing financial interests or personal relationships that could have appeared to influence the work reported in this paper.

Data availability

Data will be made available on request.

Acknowledgements

We gratefully acknowledge the financial support of the Materials Science, Energy and Nanoengineering (MSN) Department, through the Sustainable Energy Chair – ENSUS at Mohammed VI Polytechnic University (UM6P) in Morocco.

References

- [1] M.C. Hernández-Soto, A. Erigoni, C. Segarra, F. Rey, U. Díaz, E. Gianotti, I. Miletto, M. Pera-Titus, Bifunctional hybrid organosiliceous catalysts for aldol condensation – hydrogenation tandem reactions of furfural in continuous-flow reactor, *Appl. Catal. A Gen.* (2022) 118710, <https://doi.org/10.1016/j.apcata.2022.118710>.
- [2] R. Nie, Y. Tao, Y. Nie, T. Lu, J. Wang, Y. Zhang, X. Lu, C.C. Xu, Recent advances in catalytic transfer hydrogenation with formic acid over heterogeneous transition metal catalysts, *ACS Catal.* 11 (2021) 1071–1095, <https://doi.org/10.1021/acscatal.0c04939>.
- [3] K. Sytwu, M. Vadai, J.A. Dionne, Bimetallic nanostructures: combining plasmonic and catalytic metals for photocatalysis, *Adv. Phys. X* 4 (2019), <https://doi.org/10.1080/23746149.2019.1619480>.

- [4] P. Prasertpong, S. Shimpalee, N. Tippayawong, Kinetic model for esterification of oleic acid catalyzed by a green catalyst in ethanol, *Energy Rep.* 6 (2020) 66–70, <https://doi.org/10.1016/j.egyvr.2020.10.039>.
- [5] M. Mennani, M. Kasbaji, A. Ait Benhamou, A. Boussetta, Z. Kassab, M. El Achaby, N. Grimi, A. Moubarik, The potential of lignin-functionalized metal catalysts - a systematic review, *renew. Sustain. Energy Rev.* 189 (2024) 113936, <https://doi.org/10.1016/j.rser.2023.113936>.
- [6] Z. Ma, X. Xing, Z. Qu, Y. Sun, G. Sun, X. Wang, Y. Han, Activity of microporous lignin-derived carbon-based solid catalysts used in biodiesel production, *Int. J. Biol. Macromol.* 164 (2020) 1840–1846, <https://doi.org/10.1016/j.jbiomac.2020.08.002>.
- [7] X. Chen, Z. Zhang, B. Yuan, F. Yu, C. Xie, S. Yu, Lignin-based sulfonated carbon as an efficient biomass catalyst for clean benzoylation of benzene ring compounds, *J. Ind. Eng. Chem.* 111 (2022) 369–379, <https://doi.org/10.1016/j.jiec.2022.04.019>.
- [8] Z. Liu, J. Zeng, Z. Dong, Y. Chen, H. Yang, H. Chen, Insight into the mechanism of lignin amination pretreatment on lignin structure and its pyrolysis property for lignin valorization, *Chem. Eng. J.* 499 (2024) 156386, <https://doi.org/10.1016/j.cej.2024.156386>.
- [9] X. Lin, D. Chen, X. Qiu, B. Liu, J. Liu, X. Wang, S. Sun, Y. Qin, Lignin-metal supramolecular framework strategy of self-healing carbon-coated CoRu alloy nanocatalyst for efficient overall water splitting, *Adv. Energy Mater.* 14 (2024) 2303442, <https://doi.org/10.1002/aenm.202303442>.
- [10] J. Liu, L. Wu, D. Chen, Q. Xu, L. Chen, X. Lin, Y. Qin, Regulation engineering of lignin-derived N-doped carbon-supported FeNi alloy particles towards efficient electrocatalytic oxygen evolution, *Chem. Eng. Sci.* 285 (2024) 119596, <https://doi.org/10.1016/j.ces.2023.119596>.
- [11] J. Liu, J. Zhang, H. Zhou, B. Liu, H. Dong, X. Lin, Y. Qin, Lignin-derived carbon-supported MoC–FeNi heterostructure as efficient electrocatalysts for oxygen evolution reaction, *J. Colloid Interface Sci.* 629 (2023) 822–831, <https://doi.org/10.1016/j.jcis.2022.08.141>.
- [12] J. Liu, X. Qiu, S. Sun, B. Liu, Y. Tian, Y. Qin, X. Lin, Synthesis of highly dispersed carbon-encapsulated Ru–FeNi nanocatalysts by a lignin–metal supramolecular framework strategy for durable water-splitting electrocatalysis, *Green Chem.* 26 (2024) 8020–8029, <https://doi.org/10.1039/D4GC01788A>.
- [13] W. Fang, L. Liu, R. Li, R. Zhang, W. Wang, D. Zhang, Z. Cui, Preparation of bimetal-based FeNi–N/C catalyst and its electrocatalytic oxygen reduction performance, *SN Appl. Sci.* 2 (2020) 837, <https://doi.org/10.1007/s42452-020-2651-1>.
- [14] G. Qian, W. Chen, J. Chen, L.Y. Gan, T. Yu, M. Pan, X. Zhuo, S. Yin, Pyridinic-N doping carbon layers coupled with tensile strain of FeNi alloy for activating water and urea oxidation, *Green Energy Environ.* 9 (2024) 684–694, <https://doi.org/10.1016/j.gee.2022.04.006>.
- [15] S. Xu, J. Du, Q. Zhou, H. Li, C. Wang, J. Tang, Selective and leaching-resistant palladium catalyst on a porous polymer support for phenol hydrogenation, *J. Colloid Interface Sci.* 604 (2021) 876–884, <https://doi.org/10.1016/j.jcis.2021.07.067>.
- [16] L. Zhu, D. Shen, K. Hong Luo, Lignin-derived carbon quantum dots-decorated Bi7O9I3 nanosheets with enhanced photocatalytic performance: synergism of electron transfer acceleration and molecular oxygen activation, *Appl. Surf. Sci.* 608 (2023) 155273, <https://doi.org/10.1016/j.apsusc.2022.155273>.
- [17] M. Mennani, M. Kasbaji, A. Ait Benhamou, A. Boussetta, A.A. Mekkaoui, N. Grimi, A. Moubarik, Current approaches, emerging developments and functional prospects for lignin-based catalysts – review, *Green Chem.* 25 (2023) 2896–2929, <https://doi.org/10.1039/D3GC00072A>.
- [18] H. Li, W. Ma, X. Ma, M. Guo, G. Li, Multifunctional salt-assisted construction of lignin-derived Ru–co bimetal/carbon composites with rich nanointerface for electrocatalytic water splitting, *ACS Sustain. Chem. Eng.* 10 (2022) 16214–16224, <https://doi.org/10.1021/acsschemeng.2c04597>.
- [19] H. Zhou, H. Xu, Y. Liu, Aerobic oxidation of 5-hydroxymethylfurfural to 2,5-furandicarboxylic acid over Co/Mn-lignin coordination complexes-derived catalysts, *Appl. Catal. B Environ.* 244 (2019) 965–973, <https://doi.org/10.1016/j.apcatb.2018.12.046>.
- [20] R.-Y. Liu, C. Wang, B.-Z. Li, Z.-H. Liu, Y.-J. Yuan, One-pot bioconversion of lignin to 4-vinylphenol derivatives, *Chem. Eng. J.* 499 (2024) 156286, <https://doi.org/10.1016/j.cej.2024.156286>.
- [21] B. Jaleh, S. Karami, M. Sajjadi, B. Feizi Mohazzab, S. Azizian, M. Nasrollahzadeh, R.S. Varma, Laser-assisted preparation of Pd nanoparticles on carbon cloth for the degradation of environmental pollutants in aqueous medium, *Chemosphere* 246 (2020) 125755, <https://doi.org/10.1016/j.chemosphere.2019.125755>.
- [22] Y. Zhu, Z. Li, J. Chen, Applications of lignin-derived catalysts for green synthesis, *green, Energy Environ.* 4 (2019) 210–244, <https://doi.org/10.1016/j.gee.2019.01.003>.
- [23] Z. Nezafat, B. Feizi Mohazzab, B. Jaleh, M. Nasrollahzadeh, T. Baran, M. Shokouhimehr, A promising nanocatalyst: upgraded Kraft lignin by titania and palladium nanoparticles for organic dyes reduction, *Inorg. Chem. Commun.* 130 (2021) 108746, <https://doi.org/10.1016/j.inoche.2021.108746>.
- [24] O. Assila, M. Zouheir, K. Tanji, R. Haounati, F. Zerrouq, A. Kherbechi, Copper nickel co-impregnation of Moroccan yellow clay as promising catalysts for the catalytic wet peroxide oxidation of caffeine, *Heliyon* 7 (2021) e06069, <https://doi.org/10.1016/j.heliyon.2021.e06069>.
- [25] D. Ma, H. Yi, C. Lai, X. Liu, X. Huo, Z. An, L. Li, Y. Fu, B. Li, M. Zhang, L. Qin, S. Liu, L. Yang, Critical review of advanced oxidation processes in organic wastewater treatment, *Chemosphere* 275 (2021) 130104, <https://doi.org/10.1016/j.chemosphere.2021.130104>.
- [26] H.M. Ali, M.A. El-Aal, A.F. Al-Hossainy, S.M. Ibrahim, Kinetics and mechanism studies of oxidation of dibromothymolsulfonphthalein toxic dye by potassium permanganate in neutral media with the synthesis of 2-bromo-6-isopropyl-3-methyl-cyclohexa-2,5-dienone, *ACS Omega* (2022) 16109–16115, <https://doi.org/10.1021/acsomega.2c01462>.
- [27] S.M. Ibrahim, A.F. Al-Hossainy, B. Saha, M.A. El-Aal, Removal of bromothymol blue dye by the oxidation method using KMnO₄: accelerating the oxidation reaction by Ru (III) catalyst, *J. Mol. Struct.* 1268 (2022) 133679, <https://doi.org/10.1016/j.molstruc.2022.133679>.
- [28] Q. Li, A. Wang, K. Long, Z. He, R. Cha, Modified Fenton oxidation of cellulose fibers for cellulose nanofibrils preparation, *ACS Sustain. Chem. Eng.* 7 (2019) 1129–1136, <https://doi.org/10.1021/acssuschemeng.8b04786>.
- [29] Z. Tang, W. Li, X. Lin, H. Xiao, Q. Miao, L. Huang, L. Chen, H. Wu, TEMPO-oxidized cellulose with high degree of oxidation, *Polymers (Basel)* 9 (2017) 3–4, <https://doi.org/10.3390/polym9090421>.
- [30] Y. Kageshima, Y. Ojima, H. Wada, S. Koh, M. Mizuno, K. Teshima, H. Nishikiori, Insights into the electrocatalytic oxidation of cellulose in solution toward applications in direct cellulose fuel cells, *J. Phys. Chem. C* 125 (2021) 14576–14582, <https://doi.org/10.1021/acs.jpcc.1c04357>.
- [31] M. Mennani, A. Ait Benhamou, M. Kasbaji, A. Boussetta, E. Ablouh, N. Boussetta, Z. Kassab, M. El Achaby, A. Moubarik, Insights on the physico-chemical properties of alkali lignins from different agro-industrial residues and their use in phenol-formaldehyde wood adhesive formulation, *Int. J. Biol. Macromol.* 221 (2022) 149–162, <https://doi.org/10.1016/j.jbiomac.2022.08.191>.
- [32] A. Moubarik, N. Grimi, M. Boussetta, A. Pizzi, Isolation and characterization of lignin from Moroccan sugar cane bagasse: production of lignin-phenol-formaldehyde wood adhesive, *Ind. Crop. Prod.* 45 (2013) 296–302, <https://doi.org/10.1016/j.indcrop.2012.12.040>.
- [33] A. Boussetta, A.A. Benhamou, F.J. Barba, M. EL Idrissi, N. Grimi, A. Moubarik, Experimental and theoretical investigations of lignin-urea-formaldehyde wood adhesive: density functional theory analysis, *Int. J. Adhes. Adhes.* 104 (2021) 102737, <https://doi.org/10.1016/j.ijadhadh.2020.102737>.
- [34] R. Dong, Z. Yang, Y. Fu, Z. Chen, Y. Hu, Y. Zhou, H. Qin, Aminated lignin chelated metal derived bifunctional electrocatalyst with high catalytic performance, *Appl. Surf. Sci.* 580 (2022) 152205, <https://doi.org/10.1016/j.apsusc.2021.152205>.
- [35] G. Davies, J. McGregor, Hydrothermal synthesis of biomass-derived magnetic carbon composites for adsorption and catalysis, *ACS Omega* 6 (2021) 33000–33009, <https://doi.org/10.1021/acsomega.1c05116>.
- [36] S.M. Ibrahim, A.F. Al-Hossainy, Kinetics and mechanism of oxidation of bromothymol blue by permanganate ion in acidic medium: application to textile industrial wastewater treatment, *J. Mol. Liq.* 318 (2020) 114041, <https://doi.org/10.1016/j.molliq.2020.114041>.
- [37] R. Mohami, A. Shakeri, M. Nasrollahzadeh, Mannich-mediated synthesis of a recyclable magnetic kraft lignin-coated copper nanostructure as an efficient catalyst for treatment of environmental contaminants in aqueous media, *Sep. Purif. Technol.* 285 (2022) 120373, <https://doi.org/10.1016/j.seppur.2021.120373>.
- [38] Y. Abdellaoui, B. El Ibrahim, M. Ahrouch, Z. Kassab, R. El Kaim Billah, Y. Coppel, E.A. López-Maldonado, H. Abou Oualid, J.N. Díaz de León, T. Leiviskä, G. Giacomani-Vallejos, P. Gamero-Melo, New hybrid adsorbent based on APTES functionalized zeolite W for lead and cadmium ions removal: experimental and theoretical studies, *Chem. Eng. J.* 499 (2024) 156056, <https://doi.org/10.1016/j.cej.2024.156056>.
- [39] S. Chen, G. Wang, W. Sui, A.M. Parvez, L. Dai, C. Si, Novel lignin-based phenolic nanosphere supported palladium nanoparticles with highly efficient catalytic performance and good reusability, *Ind. Crop. Prod.* 145 (2020) 112164, <https://doi.org/10.1016/j.indcrop.2020.112164>.
- [40] C. Peng, Z. Kuai, X. Li, S. Lian, D. Jiang, J. Tang, L. Li, R. Wu, A. Wu, S. Chen, Facile synthesis of Ag nanoparticles/Ti3C₂Tx/polyacrylamide composite hydrogel as efficient catalyst for methylene blue and 4-nitrophenol reduction, *Mater. Des.* 210 (2021) 110061, <https://doi.org/10.1016/j.matdes.2021.110061>.
- [41] L. Serrano, E.S. Esakkimuthu, N. Marlin, M.C. Brochier-Salon, G. Mortha, F. Bertaud, Fast, easy, and economical quantification of lignin phenolic hydroxyl groups: comparison with classical techniques, *Energy Fuel* 32 (2018) 5969–5977, <https://doi.org/10.1021/acs.energyfuels.8b00383>.
- [42] J. Levanič, V.P. Šenk, P. Nadrah, I. Poljanšek, P. Oven, A. Haapala, Analyzing TEMPO-oxidized cellulose fiber morphology: new insights into optimization of the oxidation process and Nanocellulose dispersion quality, *ACS Sustain. Chem. Eng.* 8 (2020) 17752–17762, <https://doi.org/10.1021/acssuschemeng.0c05989>.
- [43] E. Toshikj, A. Tarbuk, K. Grgić, B. Mangovska, I. Jordanov, Influence of different oxidizing systems on cellulose oxidation level: introduced groups versus degradation model, *Cellulose* 26 (2019) 777–794, <https://doi.org/10.1007/s10570-018-2133-4>.
- [44] J. Yang, M. Tu, C. Xia, B. Keller, Y. Huang, F.F. Sun, Effect of fenton pretreatment on C1 and C6 oxidation of cellulose and its enzymatic hydrolyzability, *ACS Sustain. Chem. Eng.* 7 (2019) 7071–7079, <https://doi.org/10.1021/acssuschemeng.8b06850>.
- [45] M. Fodil Cherif, D. Trache, N. Brosse, F. Benaliouche, A.F., Tarchoun, comparison of the physicochemical properties and thermal stability of organosolv and kraft lignins from hardwood and softwood biomass for their potential valorization, *Waste Biomass Valoriz.* 11 (2020) 6541–6553, <https://doi.org/10.1007/s12649-020-00955-0>.
- [46] H. Yunesi-Kordkheili, Maleated lignin coreaction with phenol-formaldehyde resins for improved wood adhesives performance, *Int. J. Adhes. Adhes.* 113 (2022) 103080, <https://doi.org/10.1016/j.ijadhadh.2021.103080>.

- [47] L. Moghaddam, J. Rencoret, V.R. Maliger, D.W. Rackemann, M.D. Harrison, A. Gutiérrez, J.C. Del Río, W.O.S. Doherty, Structural characteristics of bagasse furfural residue and its lignin component. An NMR, Py-GC/MS, and FTIR study, *ACS Sustain. Chem. Eng.* 5 (2017) 4846–4855, <https://doi.org/10.1021/acssuschemeng.7b00274>.
- [48] A. Ait Benhamou, A. Boussetta, M. Nadifiyine, A. Moubarik, Effect of alkali treatment and coupling agent on thermal and mechanical properties of *Opuntia ficus-indica* cladodes fibers reinforced HDPE composites, *Polym. Bull.* (2021), <https://doi.org/10.1007/s00289-021-03619-8>.
- [49] M. Mennani, M. Kasbaji, A. Ait, A. Boussetta, Unlocking the polyfunctionality of cactus waste seed lignin in sustained catalysts: optimizing the catalytic activity of a novel maleated lignin catalyst (MLC), *Process. Saf. Environ. Prot.* 174 (2023) 433–447, <https://doi.org/10.1016/j.psep.2023.04.022>.
- [50] X. Zhang, R. Xu, Q. Liu, G. Kong, H. Lei, R. Ruan, L. Han, Enhancing the activity of Zn, Fe, and Ni-embedded microporous biocarbon: towards efficiently catalytic fast co-pyrolysis/gasification of lignocellulosic and plastic wastes, *Energy Convers. Manag.* X 13 (2022) 100176, <https://doi.org/10.1016/j.ecmx.2021.100176>.
- [51] E. Leng, Y. Guo, J. Chen, S.J.E. Liu, Y. Xue, A comprehensive review on lignin pyrolysis: mechanism, modeling and the effects of inherent metals in biomass, *Fuel* 309 (2022) 122102, <https://doi.org/10.1016/j.fuel.2021.122102>.
- [52] W.H. Arnawtee, B. Jaleh, M. Nasrollahzadeh, R. Bakshali-Dehkordi, A. Nasri, Y. Orooji, Lignin valorization: facile synthesis, characterization and catalytic activity of multiwalled carbon nanotubes/kraft lignin/Pd nanocomposite for environmental remediation, *Sep. Purif. Technol.* 290 (2022) 120793, <https://doi.org/10.1016/j.seppur.2022.120793>.
- [53] L. Azancot, L.F. Bobadilla, M.A. Centeno, J.A. Odriozola, IR spectroscopic insights into the coking-resistance effect of potassium on nickel-based catalyst during dry reforming of methane, *Appl. Catal. B Environ.* 285 (2021), <https://doi.org/10.1016/j.apcatb.2020.119822>.
- [54] Y. Wei, D. Luo, C. Zhang, J. Liu, Y. He, X. Wen, Y. Yang, Y. Li, Precursor controlled synthesis of graphene oxide supported iron catalysts for Fischer–Tropsch synthesis, *Catal. Sci. Technol.* 8 (2018) 2883–2893, <https://doi.org/10.1039/C8CY00617B>.
- [55] H. Sun, G. Wang, J. Ge, N. Wei, W. Sui, Z. Chen, H. Jia, A.M. Parvez, C. Si, Reduction of lignin heterogeneity for improved catalytic performance of lignin nanosphere supported Pd nanoparticles, *Ind. Crop. Prod.* 180 (2022) 114685, <https://doi.org/10.1016/j.indcrop.2022.114685>.
- [56] M. Arefmanesh, T.V. Vuong, J.K. Mobley, M. Alinejad, E.R. Master, M. Nejad, Bromide-based ionic liquid treatment of hardwood organosolv lignin yielded a more reactive biobased polyol, *Ind. Eng. Chem. Res.* 59 (2020) 18740–18747, <https://doi.org/10.1021/acs.iecr.0c03718>.
- [57] L. Chen, Z. Su, Q. Wu, D.H. Kuo, A.B. Abdeta, B. Wu, P. Zhang, M.T. Mosisa, O. A. Zelekew, J. Lin, X. Chen, X. Liu, Co/S co-doped Mn₃O₄-based sulfur-oxide nano-flakes catalyst for highly efficient catalytic reduction of organics and hexavalent chromium pollutants, *J. Water Process Eng.* 55 (2023) 104168, <https://doi.org/10.1016/j.jwpe.2023.104168>.
- [58] C. Linder, S.G. Rao, A. le Febvrier, G. Greczynski, R. Sjövall, S. Munktel, P. Eklund, E.M. Björk, Cobalt thin films as water-recombination electrocatalysts, *Surf. Coat. Technol.* 404 (2020) 126643, <https://doi.org/10.1016/j.surfcoat.2020.126643>.
- [59] M. Mennani, M. Kasbaji, A. Ait, E. Ablouh, Lignin-functionalized cobalt for catalytic reductive degradation of organic dyes in simple and hybrid binary systems, *Chemosphere* 350 (2024) 141098, <https://doi.org/10.1016/j.chemosphere.2023.141098>.
- [60] J. Chu, H. Ma, L. Zhang, Z. Wang, Biomass-derived paper-based nanolignin/palladium nanoparticle composite film for catalytic reduction of hexavalent chromium, *Ind. Crop. Prod.* 165 (2021) 113439, <https://doi.org/10.1016/j.indcrop.2021.113439>.
- [61] Y. Zhang, S. Ni, X. Wang, W. Zhang, L. Lagerquist, M. Qin, S. Willför, C. Xu, P. Fatehi, Ultrafast adsorption of heavy metal ions onto functionalized lignin-based hybrid magnetic nanoparticles, *Chem. Eng. J.* 372 (2019) 82–91, <https://doi.org/10.1016/j.cej.2019.04.111>.
- [62] F. Xiao, P. He, P. Yang, R. Su, Y. Wang, M. Zhao, B. Jia, Nickel-iron bimetallic sulfides nanosheets anchored on bacterial cellulose based carbon nanofiber for enhanced electrocatalytic oxygen evolution reaction, *J. Alloys Compd.* 938 (2023) 168573, <https://doi.org/10.1016/j.jallcom.2022.168573>.
- [63] T.-G. Vo, S.D.S. Hidalgo, C.-Y. Chiang, Controllable electrodeposition of binary metal films from deep eutectic solvent as an efficient and durable catalyst for the oxygen evolution reaction, *Dalton Trans.* 48 (2019) 14748–14757, <https://doi.org/10.1039/C9DT03028J>.
- [64] J.J. Liao, N.H.A. Latif, D. Trache, N. Brosse, M.H. Hussin, Current advancement on the isolation, characterization and application of lignin, *Int. J. Biol. Macromol.* 162 (2020) 985–1024, <https://doi.org/10.1016/j.ijbiomac.2020.06.168>.
- [65] M.N. Mohamad Ibrahim, N. Zakaria, C.S. Sipaut, O. Sulaiman, R. Hashim, Chemical and thermal properties of lignins from oil palm biomass as a substitute for phenol in a phenol formaldehyde resin production, *Carbohydr. Polym.* 86 (2011) 112–119, <https://doi.org/10.1016/j.carbpol.2011.04.018>.
- [66] S. Dechakumwat, P. Hongmanorom, C. Thunyaratchatanon, S.M. Smith, S. Boonyuen, A. Luengnaruemitchai, Catalytic activity of heterogeneous acid catalysts derived from corn cob in the esterification of oleic acid with methanol, *Renew. Energy* 148 (2020) 897–906, <https://doi.org/10.1016/j.renene.2019.10.174>.
- [67] H. Yu, Y. Cao, H. Li, G. Zhao, X. Zhang, S. Cheng, W. Wei, An efficient heterogeneous acid catalyst derived from waste ginger straw for biodiesel production, *Renew. Energy* 176 (2021) 533–542, <https://doi.org/10.1016/j.renene.2021.05.098>.
- [68] M. Huang, J. Luo, Z. Fang, H. Li, Biodiesel production catalyzed by highly acidic carbonaceous catalysts synthesized via carbonizing lignin in sub- and super-critical ethanol, *Appl. Catal. B Environ.* 190 (2016) 103–114, <https://doi.org/10.1016/j.apcatb.2016.02.069>.
- [69] S. Zhu, J. Luo, Z. Cheng, Y. Kuang, Q. Wu, B. Wang, W. Gao, J. Zeng, J. Li, K. Chen, Catalytic transformation of cellulose into short rod-like cellulose nanofibers and platform chemicals over lignin-based solid acid, *Appl. Catal. B Environ.* 268 (2020) 118732, <https://doi.org/10.1016/j.apcatb.2020.118732>.
- [70] A. Sandouqa, Z. Al-Hamamre, J. Asfar, Preparation and performance investigation of a lignin-based solid acid catalyst manufactured from olive cake for biodiesel production, *Renew. Energy* 132 (2019) 667–682, <https://doi.org/10.1016/j.renene.2018.08.029>.
- [71] M. Mennani, M. Kasbaji, A.A. Benhamou, A. Boussetta, E.H. Ablouh, O. Bayouf, N. Grimi, A. Moubarik, Effects of direct sulfonation on the catalytic activity and recyclability of novel lignin-based solid acid catalysts from agri-food waste, *Int. J. Biol. Macromol.* 230 (2023) 123242, <https://doi.org/10.1016/j.ijbiomac.2023.123242>.
- [72] A.A. Mekkaoui, H. Orfi, K. Bejtka, M. Laayati, S.A. Labyad, L. El Firdoussi, C. F. Pirri, A. Chiodoni, S. El Houssame, Carboxymethyl cellulose nanocolloids anchored Pd(0) nanoparticles (CMC@Pd NPs): synthesis, characterization, and catalytic application in transfer hydrogenation, *Environ. Sci. Pollut. Res.* (2022) 1–16, <https://doi.org/10.1007/s11356-022-21838-y>.
- [73] X. Zhao, P. Gao, B. Shen, X. Wang, T. Yue, Z. Han, Recent advances in lignin-derived mesoporous carbon based-on template methods, *Renew. Sustain. Energy Rev.* 188 (2023) 113808, <https://doi.org/10.1016/j.rser.2023.113808>.
- [74] J. Wang, D. Fan, L. Zhang, D. Yang, X. Qiu, X. Lin, Lignin-derived hierarchical porous carbon with high surface area and interconnected pores for efficient antibiotics adsorption, *Chem. Eng. J.* 454 (2023) 139789, <https://doi.org/10.1016/j.cej.2022.139789>.
- [75] M. Nasrollahzadeh, N. Shafiei, Z. Nezafat, N.S.S. Bidgoli, Recent progresses in the application of lignin derived (nano)catalysts in oxidation reactions, *Mol. Catal.* 489 (2020) 110942, <https://doi.org/10.1016/j.mcat.2020.110942>.
- [76] Z. Yuan, X. Shang, J. Fang, H. Li, International Journal of Biological Macromolecules A simple method for preparation of lignin / TiO₂ nanocomposites by sulfonation degree regulation and their application in polyurethane films, *Int. J. Biol. Macromol.* 198 (2022) 18–25, <https://doi.org/10.1016/j.ijbiomac.2021.12.108>.
- [77] X.F. Li, Y. Zuo, Y. Zhang, Y. Fu, Q.X. Guo, In situ preparation of K₂CO₃ supported Kraft lignin activated carbon as solid base catalyst for biodiesel production, *Fuel* 113 (2013) 435–442, <https://doi.org/10.1016/j.fuel.2013.06.008>.
- [78] R. Sandarous, B. Maleki, S. Naderi, S. Peiman, Efficient synthesis of sulfones and sulfoxides from sulfides by cobalt-based Schiff complex supported on nanocellulose as catalyst and Oxone as the terminal oxidant, *Inorg. Chem. Commun.* 148 (2023) 110294, <https://doi.org/10.1016/j.inoche.2022.110294>.
- [79] V.V. Butova, G.A. Polyakov, E.A. Erofeeva, Y.V. Rusalev, M.A. Gritsai, I. V. Ozhogin, G.S. Borodkin, D.Y. Kirsanova, Z.M. Gadzhimagomedova, A.A. Guda, A.V. Soldatov, Cobalt nanoparticles embedded in porous N-doped carbon support as a superior catalyst for the p-nitrophenol reduction, *Appl. Surf. Sci.* 592 (2022) 153292, <https://doi.org/10.1016/j.apsusc.2022.153292>.
- [80] X. Fei, Q. Xu, L. Xue, X. Zhong, Z. Zhang, K. Liu, X. Lin, T. Wang, Y. Qin, X. Qiu, Aqueous phase catalytic conversion of ethanol to higher alcohols over NiSn bimetallic catalysts encapsulated in nitrogen-doped biorefinery lignin-based carbon, *Ind. Eng. Chem. Res.* 60 (2021) 17959–17969, <https://doi.org/10.1021/acs.iecr.1c04301>.
- [81] A.A. Al-Hossainy, Combined experimental and TDDFT-DFT computation, characterization, and optical properties for synthesis of keto-bromothymol blue dye thin film as optoelectronic devices, *J. Electron. Mater.* 50 (2021) 3800–3813, <https://doi.org/10.1007/s11664-021-08955-z>.
- [82] H. Pratiwi, N. Kusmono, M.W. Wildan, Oxidized cellulose nanocrystals from durian peel waste by ammonium persulfate oxidation, *ACS Omega* 8 (2023) 30262–30272, <https://doi.org/10.1021/acsomega.3c03117>.
- [83] G. Hou, K. Chitbanyong, M. Takeuchi, I. Shibata, A. Isogai, Comprehensive study of preparation of carboxy group-containing cellulose fibers from dry-lap Kraft pulps by catalytic oxidation with solid NaOCl, *ACS Sustain. Chem. Eng.* 11 (2023) 14782–14792, <https://doi.org/10.1021/acssuschemeng.3c04750>.
- [84] A. Ait Benhamou, Z. Kassab, M. Nadifiyine, M.H. Salim, H. Sehaqui, A. Moubarik, M. El Achaby, Extraction, characterization and chemical functionalization of phosphorylated cellulose derivatives from Giant Reed Plant, *Cellulose* 28 (2021) 4625–4642, <https://doi.org/10.1007/s10570-021-03842-6>.
- [85] Z. Kassab, S. Mansouri, Y. Tamraoui, H. Sehaqui, H. Hannache, A.E.K. Qaiss, M. El Achaby, Identifying *Juncus* plant as viable source for the production of micro- and nano-cellulose fibers: application for PVA composite materials development, *Ind. Crop. Prod.* 144 (2020) 112035, <https://doi.org/10.1016/j.indcrop.2019.112035>.
- [86] M. El Achaby, Z. Kassab, A. Aboulkas, C. Gaillard, A. Barakat, Reuse of red algae waste for the production of cellulose nanocrystals and its application in polymer nanocomposites, *Int. J. Biol. Macromol.* 106 (2018) 681–691, <https://doi.org/10.1016/j.ijbiomac.2017.08.067>.
- [87] A.F. Tarchoun, D. Trache, T.M. Klöpöcke, M. Derradji, W. Bessa, Ecofriendly isolation and characterization of microcrystalline cellulose from giant reed using various acidic media, *Cellulose* 26 (2019) 7635–7651, <https://doi.org/10.1007/s10570-019-02672-x>.

- [88] Z. Belouadah, A. Ati, M. Rokbi, Characterization of new natural cellulosic fiber from *Lygeum spartum* L, *Carbohydr. Polym.* 134 (2015) 429–437, <https://doi.org/10.1016/j.carbpol.2015.08.024>.
- [89] H. Naili, A. Jelidi, O. Limam, R. Khiari, Extraction process optimization of *Juncus* plant fibers for its use in a green composite, *Ind. Crop. Prod.* 107 (2017) 172–183, <https://doi.org/10.1016/j.indcrop.2017.05.006>.
- [90] A. Ait Benhamou, A. Boussetta, Z. Kassab, M. Nadifiyine, Elaboration of carboxylated cellulose nanocrystals filled starch-based adhesives for the manufacturing of eco-friendly particleboards, *Constr. Build. Mater.* 348 (2022) 128683, <https://doi.org/10.1016/j.conbuildmat.2022.128683>.
- [91] Z. Zhang, L. Liu, H. Ma, S. Venkateswaran, B.S. Hsiao, Periodate and TEMPO sequential oxidations of cellulose fabrics: exploration of a multiple and synergistic adsorption mechanism, *Sep. Purif. Technol.* 330 (2024) 125388, <https://doi.org/10.1016/j.seppur.2023.125388>.
- [92] I. Ayouch, I. Kassem, Z. Kassab, I. Barrak, A. Barhoun, J. Jacquemin, K. Draoui, M. El Achaby, Crosslinked carboxymethyl cellulose-hydroxyethyl cellulose hydrogel films for adsorption of cadmium and methylene blue from aqueous solutions, *Surf. Interf.* 24 (2021) 101124, <https://doi.org/10.1016/j.surfin.2021.101124>.
- [93] M. Kathirselvam, A. Kumaravel, V.P. Arthanarieswaran, S.S. Saravanakumar, Characterization of cellulose fibers in *Thespesia populnea* barks: influence of alkali treatment, *Carbohydr. Polym.* 217 (2019) 178–189, <https://doi.org/10.1016/j.carbpol.2019.04.063>.
- [94] L. Azaryouh, H. Abara, Z. Kassab, E.H. Ablouh, A. Aboulkas, M. El Achaby, K. Draoui, Hybrid carbonaceous adsorbents based on clay and cellulose for cadmium recovery from aqueous solution, *RSC Adv.* 13 (2023) 6954–6965, <https://doi.org/10.1039/d2ra08287j>.
- [95] Y. Wang, D. Xiao, H. Yu, Y. Zhong, L. Zhang, X. Sui, B. Wang, X. Feng, H. Xu, Z. Mao, Composite hydrogel based oxidated sodium carboxymethyl cellulose and gelatin loaded carboxymethylated cotton fabric for hemostasis and infected wound treatment, *Int. J. Biol. Macromol.* 224 (2023) 1382–1394, <https://doi.org/10.1016/j.ijbiomac.2022.10.224>.
- [96] L. Fras, L.S. Johansson, P. Stenius, J. Laine, K. Stana-Kleinschek, V. Ribitsch, Analysis of the oxidation of cellulose fibres by titration and XPS, *Coll. Surf. Physicochem. Eng. Asp.* 260 (2005) 101–108, <https://doi.org/10.1016/j.colsurfa.2005.01.035>.
- [97] X. Lv, C. Zhao, X. Zhang, Z. Wu, L. Shuai, Preparation of aldehyde-functionalized cellulose nanocrystals via aerobic oxidation of cellulose in a recyclable triisopropoxy vanadium oxidation system††Electronic supplementary information (ESI) available, *Green Chem.* 26 (2024) 1876–1882, <https://doi.org/10.1039/d3gc04583h>.
- [98] S. Zulkepli, N. Abd. Rahman, H. Voon Lee, C. Kui Cheng, W.-H. Chen, J. Ching Juan, Synergistic effect of bimetallic Fe-Ni supported on hexagonal mesoporous silica for production of hydrocarbon-like biofuels via deoxygenation under hydrogen-free condition, *Energy Convers. Manag.* 273 (2022) 116371, <https://doi.org/10.1016/j.enconman.2022.116371>.
- [99] H. Liang, Q. Zhao, S. Liu, C. Wei, Y. Wang, Y. Wang, S. Huang, X. Ma, Synergistic effect of Fe-Mn bimetallic sites with close proximity for enhanced CO₂ hydrogenation performance, *Front. Chem. Sci. Eng.* 18 (2024) 140, <https://doi.org/10.1007/s11705-024-2491-4>.
- [100] J. Li, Y. Qin, T. Tan, Q. Zhu, B. Ouyang, E. Kan, W. Zhang, Enhancing the activity of FeNi bimetallic electrocatalysts on overall water splitting by Nd₂O₃-induced FeNi lattice contraction, *J. Energy Chem.* 87 (2023) 42–50, <https://doi.org/10.1016/j.jechem.2023.08.021>.
- [101] M. Dmitry Yu, S. Tapio, *Catalytic Kinetics*, Chapter 2, 2016, pp. 35–100, <https://doi.org/10.1016/b978-0-444-63753-6.09994-2>.
- [102] B. Changmai, P. Sudarsanam, L. Rokhum, Biodiesel production using a renewable mesoporous solid catalyst, *Ind. Crop. Prod.* 145 (2020) 111911, <https://doi.org/10.1016/j.indcrop.2019.111911>.
- [103] Z. Dou, Y. Zhang, Z. Li, Z. Fang, H. Li, J. Fang, One-step preparation of lignin-based solid acid by carbonization and sulfonation to catalyze the synthesis of dimethyl adipate, *Ind. Crop. Prod.* 180 (2022) 114721, <https://doi.org/10.1016/j.indcrop.2022.114721>.
- [104] M.F. Hussein, A.O. Abo El Naga, M. El Saied, M.M. AbuBaker, S.A. Shaban, F.Y. El Kady, Potato peel waste-derived carbon-based solid acid for the esterification of oleic acid to biodiesel, *Environ. Technol. Innov.* 21 (2021) 101355, <https://doi.org/10.1016/j.eti.2021.101355>.
- [105] B. Zhang, M. Gao, J. Geng, Y. Cheng, X. Wang, C. Wu, Q. Wang, S. Liu, S. M. Cheung, Catalytic performance and deactivation mechanism of a one-step sulfonated carbon-based solid-acid catalyst in an esterification reaction, *Renew. Energy* 164 (2021) 824–832, <https://doi.org/10.1016/j.renene.2020.09.076>.
- [106] C.H. Bartholomew, Mechanisms of catalyst deactivation, *Appl. Catal. A Gen.* 212 (2001) 17–60, [https://doi.org/10.1016/S0926-860X\(00\)00843-7](https://doi.org/10.1016/S0926-860X(00)00843-7).
- [107] Y. Li, D. Nishu, C. Yellezuome, R. Liu Li, Deactivation mechanism and regeneration effect of bi-metallic Fe-Ni/ZSM-5 catalyst during biomass catalytic pyrolysis, *Fuel* 312 (2022) 122924, <https://doi.org/10.1016/j.fuel.2021.122924>.
- [108] M. Rahmati, M.-S. Safdari, T.H. Fletcher, M.D. Argyle, C.H. Bartholomew, Chemical and thermal sintering of supported metals with emphasis on cobalt catalysts during fischer–tropsch synthesis, *Chem. Rev.* 120 (2020) 4455–4533, <https://doi.org/10.1021/acs.chemrev.9b00417>.
- [109] A.J. Martín, S. Mitchell, C. Mondelli, S. Jaydev, J. Pérez-Ramírez, Unifying views on catalyst deactivation, *Nat. Catal.* 5 (2022) 854–866, <https://doi.org/10.1038/s41929-022-00842-y>.